Mode coupling for precise measurements of the electronic g-factor of hydrogen-like ions in Penning traps

Tristán Valenzuela Salazar
geb. in Saint Maurice (Frankreich)
Mainz, im Juni 2004

Berichterstatter der Arbeit: Prof. Dr.
                                 Prof. Dr.
Datum der mündlichen Prüfung: 05.08.2004

A Marisa y Black

Contents

Chapter 1

Introduction

1.1 The *g-factor*

A current I flowing in a closed loop (fig. 1.1) has an associated magnetic moment
in the form of

$$\vec{\mu} = \frac{I}{2} \oint \vec{r} \times d\vec{\ell} = I\vec{A} \tag{1.1}$$

where $d\vec{\ell}$ is the element of loop, $\vec{r}$ is its position's vector and $\vec{A}$ is the area vector
corresponding to the area enclosed in the loop. According to this definition, for a
classical charged particle orbiting with angular momentum $\vec{L}$ its magnetic moment
can be expressed as

$$\vec{\mu}_l = \frac{q}{2m}\vec{L} \tag{1.2}$$

where q and m are the particle's charge and mass respectively. This can be gener-
alized for a quantum particle with total angular momentum $\vec{J} = \vec{L} + \vec{S}$, where $\vec{S}$
denotes the spin and $\vec{L}$ the mechanical angular momentum. In this case, a dimen-
sionless constant g_J has to be introduced which is a function of the total angular
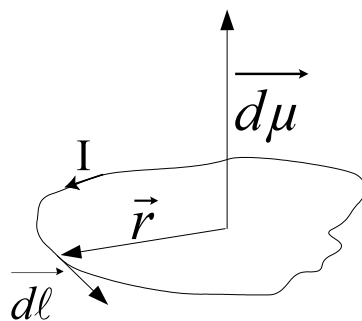

Figure 1.1: **Elementary magnetic dipolar moment created by an element
of current loop $d\vec{\ell}$ at a position $\vec{r}$ from the origin of coordinates**

momentum $\vec{J}$, to be able to reproduce the classical results. This constant is called Landé's gyromagnetic factor or, for simplicity, the *g-factor*. The magnetic moment is then, in general,

$$\vec{\mu}_J = g_J \frac{q}{2m} \vec{J} \tag{1.3}$$

where g_J is given by Landé's formula

$$g_J = \frac{3}{2} + \frac{s(s+1) - l(l+1)}{2j(j+1)} \tag{1.4}$$

Thus, for a free particle with spin $s = \frac{1}{2}$ the *g-factor* (in this case g_s) should be $g_s = 2$. From now on we will discuss the electronic magnetic moment that is $\vec{\mu}_e = -g_J \mu_B \vec{J}$, where μ_B is the so-called Bohr magneton given by $\mu_B = e/2m_e$, with e being the elementary charge and m_e the electron's mass. For the free electron the *g-factor* is supposed to be exactly 2 but due to relativistic and quantum electrodynamical effects it deviates from this value at the 10^{-3} level. The most precise experiment on the free electronic *g-factor* performed by Dehmelt and coworkers [Deh87] gave a result for the so-called *g-factor anomaly* of

$$a_e = \frac{g-2}{2} = 0.001\ 159\ 652\ 188\ 4(43). \tag{1.5}$$

In order to perform theoretical predictions, the rules of perturbative quantum electrodynamics (QED) are applied to the system under consideration. Interactions between Dirac particles with charges $\pm e$ are mediated by exchange of photons. Each exchanged photon introduces a factor α in the corresponding matrix element, α being the fine structure constant ($\alpha \approx 1/137$). Therefore, a perturbation expansion for the interaction between particles and for the radiative corrections is possible. The radiative corrections consist of the self energy, the vacuum polarization and the vertex corrections (fig. 1.2).

Figure 1.2: The basic quantum electrodynamical processes, represented as Feynman diagrams. The plain lines denote free electrons or positrons, the curly lines denote photons. (a) Emission and reabsorption of a virtual photon by an electron, the so-called *self energy*. (b) Creation and re-annihilation of a virtual electron-positron pair by a photon, the so-called *vacuum polarization*. (c) Modification of a basic electron-photon interaction by an additional virtual photon, the so-called *vertex correction*.

Then the *g-factor* can be expressed as a series expansion of the radiative term in powers of the fine structure constant α:

$$g_{free} = 2 \Big(\sum_{n=0}^{\infty} A_{2n} \Big(\frac{\alpha}{\pi} \Big)^n + A(\mu, \tau, hadronic) \Big) \tag{1.6}$$

In the term $A(\mu, \tau, hadronic)$ all the contributions from heavier leptons, hadrons and weak interactions are included. The terms in $(\frac{\alpha}{\pi})^0, (\frac{\alpha}{\pi})^1, (\frac{\alpha}{\pi})^2, (\frac{\alpha}{\pi})^3$ have analytical expressions and the term in $(\frac{\alpha}{\pi})^4$ can be calculated numerically. This calculation up to the order $(\frac{\alpha}{\pi})^4$ was performed by Kinoshita [Kin90] yielding

$$
\begin{aligned}
A_0 &= 1, \\
A_2 &= 0.5, \\
A_4 &= -0.328\ 478\ 965\ldots, \\
A_6 &= 1.181\ 241\ 456\ldots, \\
A_8 &= -1.509\ 8(384), \\
A(\mu, \tau, hadronic) &= 4.939(27) \cdot 10^{\ 12}.
\end{aligned}
\tag{1.7}
$$

As a result of the series expansion the value of the theoretical *g-factor* is depending on the value of the fine structure constant. In [Hug99] Hughes and Kinoshita took into account four different values of α coming from independent experiments (Quantum Hall effect, ac Josephson effect, muonium hyperfine structure and the *de Broglie* wavelength of a neutron beam). The weighted average of these results gives a value for the theoretical *g-factor* anomaly of

$$
a_e(theory) = 0.001\ 159\ 652\ 187\ 2(449)
\tag{1.8}
$$

which is in perfect concordance with the experimental result. This is one of the most stringent QED test. Furthermore, assuming the validity of the QED calculations the measurement of the *g-factor* anomaly for the free electron could yield an independent result for the fine structure constant α.

1.2 The bound state corrections to the electronic *g-factor*

The recent increase of interest on QED in presence of strong fields makes it necessary to investigate a way to create such strong fields and how they interact with electrons. In atomic systems the inner electrons are in a region of high electric field created by the nucleus, as can be seen in fig. 1.3. For the $1S_{1/2}$ electron in high nuclear charge (Z) atoms the field strength is close to the critical value, which is the one at which an electron-positron pair is created spontaneously. For an homogeneous field this critical value amounts to [Sch51, Sch54a, Sch54b]

$$
E_{crit} = \frac{(m_e c^2)^2}{e\hbar c} = 1.323 \times 10^{16}\ V/cm.
\tag{1.9}
$$

In order to perform a high field QED test in atomic systems the first thing to do is to evaluate which is the most convenient atomic phenomenon to investigate. There are three interesting quantities to study, namely the hyperfine splitting, the binding energies and the Zeeman splitting (directly related to the electronic g_J factor). Attending to the expected value of the characteristic radial dependence of the operators related to these quantities, which are $\langle 1/r^2 \rangle$, $\langle 1/r \rangle$ and $\langle r \rangle$ (fig. 1.4) respectively one tends to choose the Zeeman splitting since it is the less affected by nuclear effects. In an atomic ion the spin is not a good quantum number anymore, the only angular
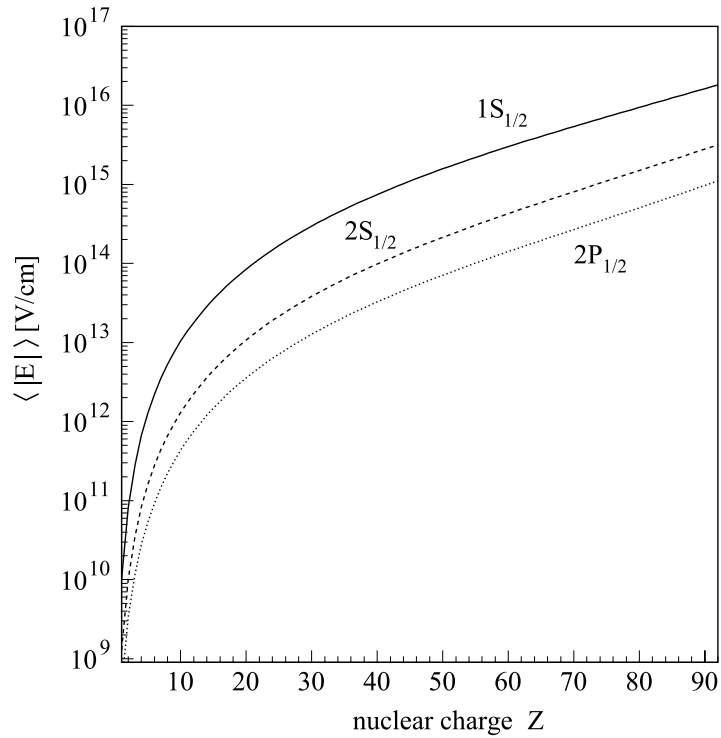
Figure 1.3: **Expectation value of the electrical field strength for the lowest-lying states of a hydrogen-like atom in the range Z=1-92. Figure from [Bei00].**

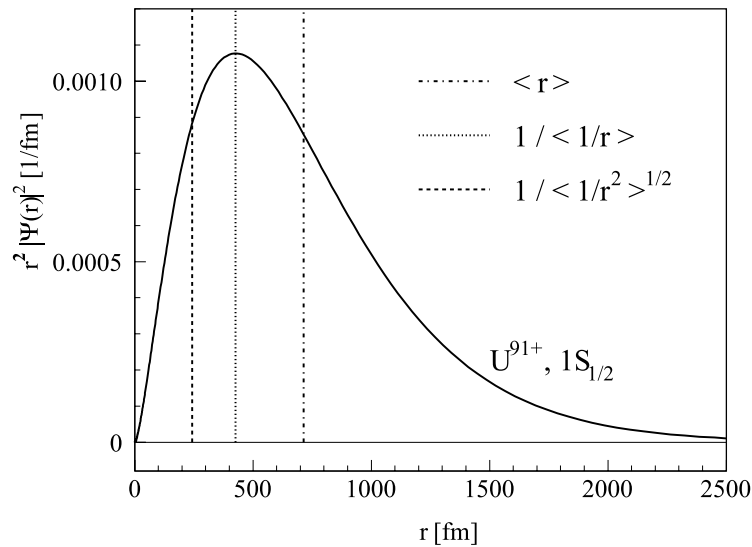Figure 1.4: **Probability density of the** $1S_{1/2}$**-state wave function. Some characteristic expectation values are also indicated, where** $\langle 1/r^2 \rangle$ **reflects the characteristic radial dependence of the hyperfine structure splitting operator,** $\langle 1/r \rangle$ **that of the binding energy and** $\langle r \rangle$ **that of the Zeeman effect and thus the** g_J **factor. Figure from [Bei00].**

momentum related quantum number is the total angular momentum J. Thus, it makes no sense to talk about the *g-factor* related to the electronic spin but the g_J factor of the ion. But in the special case of a nucleus with vanishing angular momentum (e.g. even-even nucleus) and striped of all its electrons but one, the total angular momentum of the ion coincides with the one of the electron, and if the electron is in the $1S_{1/2}$ state, it coincides with the electron spin. Such an ion with only one electron in the $1S_{1/2}$ state is what is usually called a hydrogen-like ion because its electronic cloud is the same than the one of the neutral hydrogen. Another interesting feature of hydrogen-like ions is that all the atomic properties are much easier to calculate than in other ions due to the simplicity of having only one electron and therefore there is no electronic shielding or electron-electron interaction. All these facts make the g_J factor of hydrogen-like ions a suitable quantity for bound state QED tests.

The correct description of the bound electron is obtained through the solution of Dirac's equation. The first attempt was performed by Breit [Bre28] who derived the equation

$$g_J = 2 \left[\frac{1 + 2\sqrt{1 - (Z\alpha)^2}}{3} \right]. \tag{1.10}$$

This solution is only valid for pointlike nuclei. It is a full relativistic solution but does not take into account any correction due to QED-effects. The extension of the nucleus implies a small modification in the electronic wave function, which leads to a deviation in the *g-factor* of the $1S_{1/2}$ electron that spreads from below 1.0×10^{-11} for ^{1}H and ^{4}He up to more than 1.0×10^{-3} for ^{232}Th,^{238}U and ^{244}Pu [Bei00]. As a result a different approach is needed in order to get closer to a realistic solution. The common way is to try to make a series expansion in the same way as for the free electron, but now, the interaction with the binding potential has to be taken into account. The *g-factor* of an electron bound in a hydrogen like ion can be expressed

	^{12}C^{5+}	^{16}O^{7+}
Dirac Value (point)	1.998 721 354 4	1.997 726 003 1
Fin. nucl. size	0.000 000 000 4	0.000 000 001 5
QED, order (α/π)	0.002 323 663 7(9)	0.002 324 416(1)
QED, order $(\alpha/\pi)^2$	-0.000 003 516 2(2)	-0.000 003 517 1(4)
Recoil	0.000 000 087 6	0.000 000 117 0
Total	2.001 041 589 9(9)	2.000 047 021(1)

	^{40}Ca^{19+}	^{238}U^{91+}
Dirac Value (point)	1.985 723 203 8(1)	1.654 846 173(3)
Fin. nucl. size	0.000 000 113 1(1)	0.001 275 0(25)
QED, order (α/π)	0.002 336 92(1)	0.003 088 93(3)
QED, order $(\alpha/\pi)^2$	-0.000 003 528(9)	-0.000 003 8(9)
Recoil	0.000 000 297 1	0.000 002 491
Total	1.988 057 01(2)	1.659 208 9(27)

Table 1.1: **Contributions to the $1S_{1/2}$ bound-electron *g-factor* in hydrogen like carbon, oxygen, calcium and uranium. Table extracted from [Yer02].**

as

$$g_{j1s_{1/2}}(Z) = 2\left[C^{(0)} + C^{(2)}\left(\frac{\alpha}{\pi}\right) + C^{(4)}\left(\frac{\alpha}{\pi}\right)^2 + C^{(6)}\left(\frac{\alpha}{\pi}\right)^3 + C^{(8)}\left(\frac{\alpha}{\pi}\right)^4 + \dots\right] \quad (1.11)$$

where $C^{(0)}$ contains the Dirac *g-factor* of the free electron as well as the correction due to the binding but none of the QED corrections, and is given by the so-called Breit Formula (eq. 1.10). The factors $C^{(2n)}$ can be obtained by adding to the free electron coefficients A_{2n} (eq. 1.6) the QED binding effects. To calculate the QED binding effects it has to be taken into account that now the coupling constant for the interaction between the electron and the nucleus is dependent on the nuclear charge Z and is therefore of magnitude $Z\alpha$. Thus, the QED binding term can be expanded in a series in $Z\alpha$ whose leading term is given by

$$C^{(2)} = \frac{1}{2} + \frac{(Z\alpha)^2}{12} + \dots \quad (1.12)$$

Bound QED corrections in order $(\alpha/\pi)^2$ have not yet been calculated. An estimation can be obtained observing that all coefficients A_{2n} in eq. 1.6 are of magnitude 1. Therefore, it is reasonable to assume a scaling by factor (α/π) also for the bound state contributions. The most accurate estimation, up to now, was performed by V.A. Yerokhin *et al.* [Yer02]. In table 1.1 the theoretical values for some ions are presented as an example.

As tests to these theoretical approaches a number of experiments have been performed during the last years. Table 1.2 shows some of the most prominent results and the comparison with the theoretical prediction.

	g_j(experiment)	g_j(theory)	Method	Ref.
^{1}H	2.002 283 845(26)	2.002 283 853	SEOP[1]	[Tie77]
^{4}He$^+$	2.002 177 4(60)	2.002 177 407	SEOP	[Joh80]
^{12}C^{5+}	2.001 042(2)	2.001 041 591(7)	PT[2]	[Her00]
^{12}C^{5+}	2.001 041 596(5)	2.001 041 591(7)	PT	[Häf00b]
^{16}O^{7+}	2.000 047 025 4(46)	2.000 047 021(1)	PT	[Ver04]
^{207}Pb^{81+}	1.78(12)	1.738 281 14	HFST [3]	[See98]
^{209}Bi^{82+}	1.734 1(35)	1.731 013 38	HFST	[Win99]

Table 1.2: **Some experimental g-factor values for several ions and the theoretical prediction.**

The goal of the present work is to discuss the experiments performed with the Penning trap technique and to propose an improvement of this technique. This improvement consist on reducing the systematical uncertainties arising from the finite energy of the particles under study by a measurement technique that does not need the motions to be excited, as has been required until now.

---

[1]Spin-Exchange Optical Puming

[2]Penning Trap technique, is based on the measurement of the Larmor precession frequency of the spin of an ion confined in space. The magnetic field is calibrated through the measurement of the ion's cyclotron frequency

[3]Hyperfine Splitting Transition

Chapter 2

Theoretical aspects

2.1 Trapping of charged particles

According to Heisenberg's uncertainty principle, $\Delta E \Delta t \geq \hbar$, a long observation time is needed in order to be able to perform high precision measurements of energies. To achieve long observation times it is important to have the experimental object localized in space. In order to get this confinement for charged particles it is natural to think in combinations of electromagnetic fields. According to the Laplace equation $\Delta \phi = 0$, in absence of charges, it is not possible to create a 3-dimensional potential minimum with the only help of electrostatic fields. To overcome this problem, mainly, two possible solutions have been developed :

- The Paul traps: achieving a time averaged potential minimum by adding a rotating quadrupolar AC-field.

- The Penning traps: generate a potential minimum in one direction (z-axis) and confine in the perpendicular direction by means of an homogeneous magnetic field in the direction of the z-axis ($\vec{B} = B\vec{u_z}$).

For the present experiment the second solution was chosen. For very precise measurements it is convenient to have linear forces for the motion forming a combination of harmonic oscillators. The typical way to achieve this kind of potential is to use electrodes with the shape of revolution hyperboloids (fig 2.1) following the curves given by

$$z^2 = {z_0}^2 + \rho^2/2$$
$$z^2 = \frac{1}{2}(\rho^2 - {\rho_0}^2).$$

This electrode geometry gives rise to a quadrupolar potential of the form $U = \frac{U_0}{2d^2}(z^2 - \frac{\rho^2}{2})$, where z and ρ are the cylindrical coordinates, $d = \frac{1}{2}({z_0}^2 + {\rho_0}^2/2)$ is the so-called

trap parameter with z_0 and ρ_0 being the minimum distances of the hyperbolas to the origin in the axial and radial directions respectively, and U_0 is the voltage applied between the electrodes. In this potential and with a superimposed homogeneous
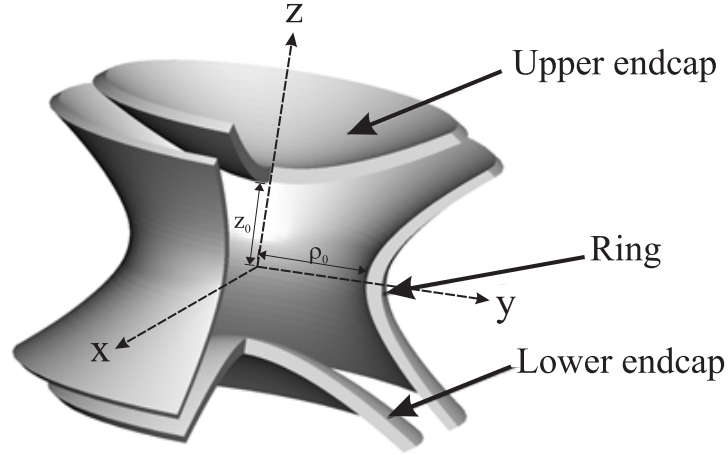

Figure 2.1: **Set of hyperbolical electrodes which compose the classical Penning trap. Indicated are the characteristic lengths z_0 and ρ_0.**

magnetic field in the z direction, a charged particle "sees" a Lorentz force:

$$\vec{F} = q(\vec{E} + \vec{v} \times \vec{B}) \tag{2.1}$$

since $\vec{B} = B\vec{u}_z \Rightarrow \vec{v} \times \vec{B} \perp \vec{u}_z$. The so-called axial motion is decoupled from the magnetic field, and is given by

$$\ddot{z} = -\frac{qU_0}{md^2}z \tag{2.2}$$

which corresponds to a simple harmonic oscillator of frequency

$$\omega_z = \sqrt{\frac{qU_0}{md^2}}. \tag{2.3}$$

On the other hand, the motion in the x-y-plane is given by

$$\ddot{x} = \frac{q}{m}(B\dot{y} - \frac{U_0}{2d^2}x) \tag{2.4a}$$

$$\ddot{y} = -\frac{q}{m}(B\dot{x} + \frac{U_0}{2d^2}y). \tag{2.4b}$$

Introducing the variable $u = x + iy$ and replacing the expression of the free particle cyclotron frequency, $\omega_c = \frac{q}{m}B$, the equation of motion becomes

$$\ddot{u} + \omega_c\dot{u} + \frac{\omega_z{}^2}{2}u = 0. \tag{2.5}$$

This can easily be solved, yielding the solution of two decoupled harmonic oscillators of frequencies

$$\omega_+ = \frac{\omega_c}{2} + \sqrt{\frac{\omega_c{}^2}{4} - \frac{\omega_z{}^2}{2}} \tag{2.6a}$$

$$\omega = \frac{\omega_c}{2} - \sqrt{\frac{\omega_c{}^2}{4} - \frac{\omega_z{}^2}{2}}. \tag{2.6b}$$

They are the so-called reduced cyclotron and magnetron frequency, respectively. The motion has then the shape shown in figure 2.2.
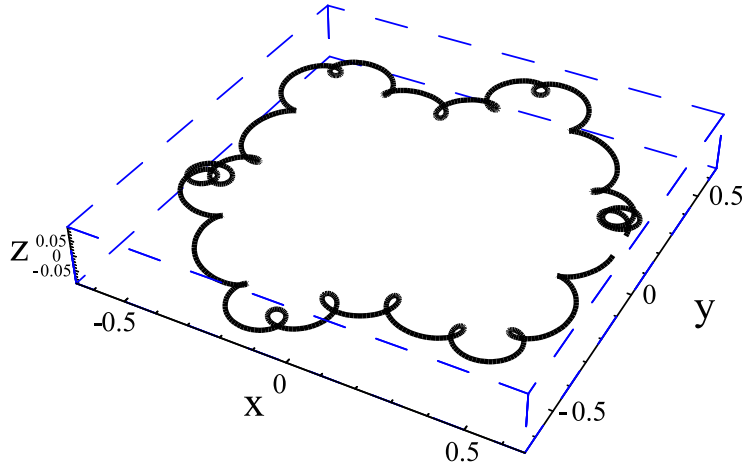

Figure 2.2: **Example of motion of an ion in a Penning trap. All lengths are expressed in arbitrary units.**

In the present experiment one eventually needs to load ions from outside and to introduce microwaves, so the cylindrical geometry proposed by Gabrielse *et al.* [Gab89] is used and will be discussed in the section 2.1.2.

2.1.1 Quantum mechanical description of the motion

In general the motion of an ion in a trap can be perfectly described in terms of classical mechanics due to the relatively high energies involved. But nevertheless for some details it will be needed to some extent to take into account the quantized character of the motion. Therefore a summary of the most important features of the quantum mechanical description of the motion will be presented. As explained above, the motion of a charged particle in the trap is the composition of three harmonic oscillators, so a detailed description of the quantized harmonic oscillator follows.

The motion in the ideal Penning trap

For describing the motion of a charged particle in a Penning trap in terms of the Quantized Harmonic Oscillator (Q.H.O.) the corresponding ladder operators have to be introduced for the different degrees of freedom. For the axial motion, as it is decoupled from all the other degrees of freedom it is a simple one dimensional Q.H.O and the definition of the ladder operators is as follows

$$a_z = \sqrt{\frac{m\omega_z}{2\hbar}}(z + i\frac{p_z}{m\omega_z}) \tag{2.7a}$$

$$a_z^{\dagger} = \sqrt{\frac{m\omega_z}{2\hbar}}(z - i\frac{p_z}{m\omega_z}) \tag{2.7b}$$

For the description of the motion in the radial plane the two motions have to be decoupled. This is done by introducing an auxiliary operator V in such a way that the equation of motion gets decoupled. This operator is defined as

$$V = \frac{\partial}{\partial t}\rho - \omega \; \hat{z} \times \rho \tag{2.8}$$

Then the ladder operators can be constructed as

$$a = \sqrt{\frac{m}{2\hbar(\omega_+ - \omega)}}(V_x \mp iV_y) \tag{2.9a}$$

$$a^{\mathbf{y}} = \sqrt{\frac{m}{2\hbar(\omega_+ - \omega)}}(V_x \pm iV_y)) \tag{2.9b}$$

Now, from the definitions in eqs. 2.7, 2.9, the Hamiltonian can be written as

$$H = \hbar\omega_z(N + 1/2) + \hbar\omega_+(K + 1/2) - \hbar\omega \; (L + 1/2) \tag{2.10}$$

So the energy eigenvalues are given by

$$E = \hbar\omega_z(n + 1/2) + \hbar\omega_+(k + 1/2) - \hbar\omega \; (l + 1/2) \tag{2.11}$$

where the unstable character of the magnetron motion can be seen from the negative sign of its energy component. The confinement in the Penning trap is only possible due to the extremely long time constant of the radius growing in the magnetron motion.
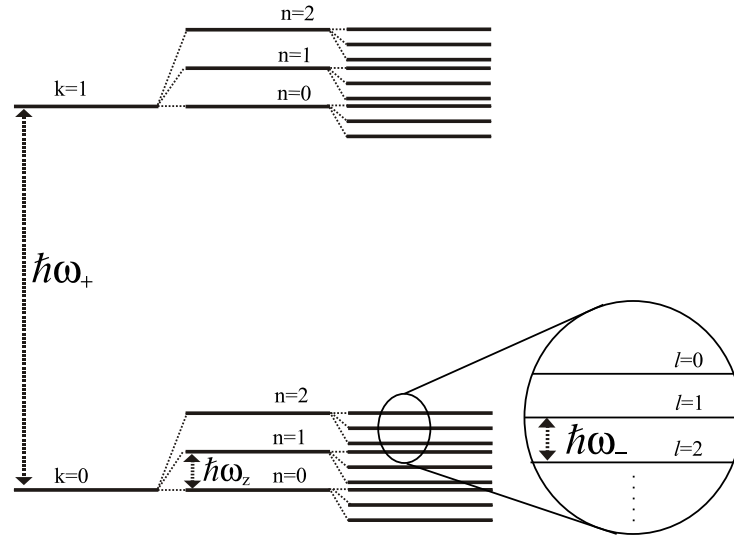

Figure 2.3: **Energy eigenvalues of the three Quantum Harmonic Oscillators of a charged particle stored in a Penning trap. The energy gap between levels is proportional to the frequencies of each degree of freedom. The ratios of the frequencies of a $^{12}C^{5+}$ ion in our setup are 25:1:0.015 $(\omega_+ : \omega_z : \omega$). The gaps in the figure are scaled to these ratios, except for the magnetron motion, which is magnified 20 times for a better visibility.**

2.1.2   Open-endcap cylindrical double Penning trap

In the present experiment this solution was adopted in order to be able to

- create ions outside of the trap

- create a well-known microwave field

The trap electrodes have no longer hyperbolical shape but they are open cylinders. This geometry is chosen because it makes easier to calculate the microwave field distribution and also simplifies the introduction of ions from the outside. Another advantage of this geometry is the better mechanical accuracy that can be achieved while machining the metallic pieces.
To minimize the anharmonicities arising from the deviation of the hyperbolical shape, the trap is composed of five electrodes instead of three: one ring and two endcaps plus two correction electrodes (fig. 2.4) intended to make the potential harmonic in a region as big as possible.
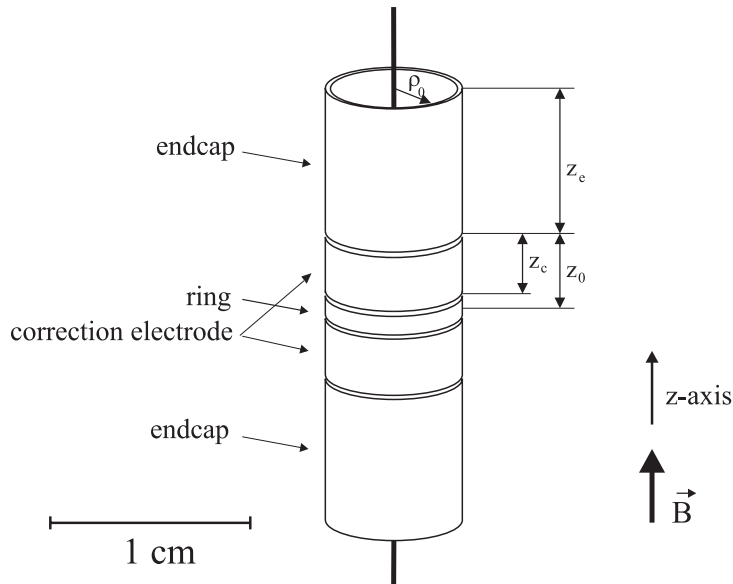

Figure 2.4: **Sketch of a cylindrical trap**

Generally, for a non-perfect set of electrodes the created potential is no longer harmonic, but anyways, for the present geometry, i.e assuming cylindrical symmetry and axial symmetry under reflection across the $z = 0$ plane, the potential can be expressed as a series expansion in terms of Legrendre polynomials

$$U = \frac{U_0}{2} \sum_{k=0}^{\infty} C_{2k} \left(\frac{r}{d}\right)^{2k} P_{2k}(\cos \theta) \tag{2.12}$$

where r and θ are the spherical coordinates. Even terms are non-vanishing because of the already mentioned azimuthal symmetry. From eq. 2.12 one can see that for a perfectly harmonic potential only the term $k = 1$ makes a contribution . The term with $k = 0$ which contributes only with an overall offset of the potential is disregarded. If $d = \frac{1}{2}(z_0{}^2 + \rho_0{}^2/2)$, then $C_2 = 1$ (z_0 and ρ_0 are defined in fig. 2.4).

Then, to the lowest order, the axial oscillation frequency ω_z of a particle of mass m and charge q is given by

$$\omega_z = \sqrt{\frac{qU_0C_2}{md^2}}.\tag{2.13}$$

If $C_4 \neq 0$ the potential is no longer harmonic and the frequency depends on the amplitude of the oscillation. The shift in the axial frequency can be written [Bro86, Gab89] as

$$\frac{\Delta\omega_z}{\omega_z} = \frac{3}{2}\left(\frac{C_4}{C_2}\right)\frac{E_z}{qU_0C_2}\tag{2.14}$$

where E_z is the axial energy of the charged particle.

An important task is then to minimize the frequency shifts due to the trap anharmonicities, to first order, this means to minimize C_4. This is where the correction electrodes come into play. If a potential U_0 is applied between the ring and the endcaps and a potential U_c between the correction electrodes and the endcaps, the potential can be written as a superposition $U = U_{ring} + U_{corr}$ where U_{ring} and U_{corr} are the potentials created by the ring and the correction electrodes, respectively. In a small region near the center of the trap, U_{ring} and U_{corr} are the solutions to the Laplace equation with boundary conditions as sketched in fig. 2.5, and they take the form:

$$U_{ring} = \frac{U_0}{2}\sum_{k=0}^{\mathbf{1}} C_k{}^{(c)}\left(\frac{r}{d}\right)^k P_k(\cos\theta)\tag{2.15a}$$

$$U_{corr} = \frac{U_c}{2}\sum_{k=0}^{\mathbf{1}} D_k\left(\frac{r}{d}\right)^k P_k(\cos\theta).\tag{2.15b}$$
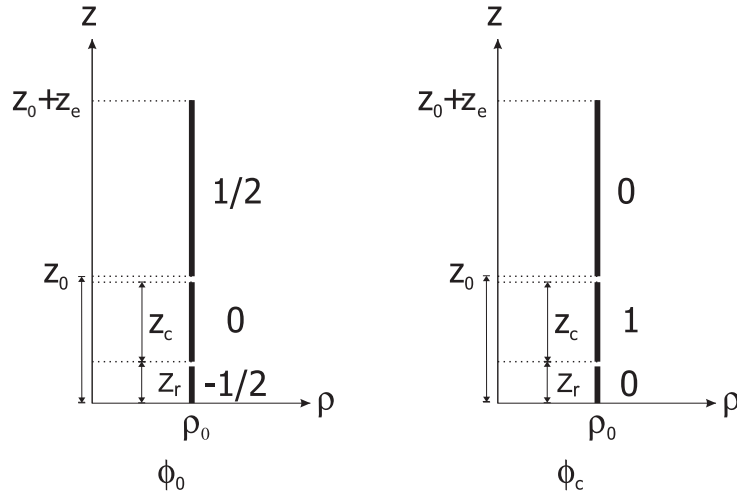

Figure 2.5: **Boundary conditions for solutions of Laplace's equation for two contributions of the potential in a corrected cylindrical Penning trap. Both are symmetric under rotations around the z-axis and under reflections across the plane $z = 0$.**

By comparison of eq. 2.15 with eq. 2.12, the coefficients C_k can be rewritten as

$$C_k = C_k^{(c)} + D_k \frac{U_c}{U_0}. \tag{2.16}$$

The fraction U_c/U_0 will be from now on called "Tuning-ratio" (TR).
The coefficients $C_k^{(c)}$ and D_k are functions only of the trap's geometry, so for a given geometry it is possible to choose a TR such that C_4 vanishes:

$$\left(\frac{U_c}{U_0}\right)_{C_4=0} = \frac{-C_4^{(c)}}{D_4}. \tag{2.17}$$

But, in general, this adjusting of the tuning-ratio acts also on the C_2-term and therefore in the axial frequency ω_z, leading to a new search of the axial resonance for every change in the tuning-ratio. To overcome this problem, G. Gabrielse [Gab89] proposes a so-called orthogonalized trap: a geometry such that D_2 vanishes. Then, tuning the trap to make $C_4 = 0$ will have no effect on C_2 and therefore also not on ω_z. In our case, the geometry was chosen such that D_2 vanishes, but in fact there is a small deviation from the orthogonality because the finite accuracy of the manufacture of the electrodes . With the actual geometrical parameters of our trap (table 2.1), a value of $D_2 = (-1.594 \pm 0.002)10^{-3}$ mm^{-2} is obtained and from there the dependency of the axial frequency with the tuning-ratio is found to be

$$\frac{\partial \omega_z}{\partial TR} = \frac{qU_0}{m\omega_z} D_2 = 23.8 \text{ Hz/mUnit}^{[1]} \tag{2.18}$$

for an ion of hydrogen-like carbon $^{12}\text{C}^{5+}$.

Object	Magnitude [mm]
Endcap	z_e=6.80
Ring	z_r=0.92
Correction electrodes	z_c=0.92
Radius	ρ_0=3.50
Gap between electrodes	d=0.14

Table 2.1: **Dimensions of the trap electrodes**

2.2   Magnetic bottle

In order to determine the g-factor, the Larmor precession frequency of the electronic spin in a magnetic field has to be measured. In order to achieve this goal the spin degree of freedom of the trapped particles has to be observable. In the case of our setup this is achieved by coupling the spin degree of freedom with the axial motion, which can be induced through an inhomogeneity in the magnetic field. This inhomogeneity is created by introducing a piece of ferromagnetic material in the trap. Actually, in order to keep the maximum symmetry the ring electrode of the trap is made of nickel. This nickel ring distorts the magnetic field lines of the

---

[1]mUnit $\equiv \triangle TR = 0.001$

otherwise homogeneous magnetic field. Therefore, the magnetic field has now not only an axial component but also some radial component and thus can be written as $\vec{B} = B_\rho \cdot \vec{u}_\rho + B_z \cdot \vec{u}_z$. Nevertheless, it can be shown [Ver03] that the ratio B_ρ/B_z is small. Therefore, only the axial part of the magnetic field B_z will be taken into account. Anyway, B_z is not a constant but is position dependent $B_z = B_z(\rho, z)$ due to the inhomogeneity. On the z axis, $\rho = 0$, the magnetic field strength can be written as a series expansion

$$B = \sum_{n=0}^{\boldsymbol{1}} B_n z^n \qquad (2.19)$$

where only the even terms are taken into account due to the rotational symmetry around the z-axis and

$$B_{2k} = \frac{1}{2k!} \frac{\partial^{2k}}{\partial z^{2k}} B_z(\rho, z) \bigg|_{(0, z_0)}. \qquad (2.20)$$

Assuming a sufficiently small inhomogeneity, in our case $B_2/B_0 < 3 \cdot 10^{-3} mm^{-2}$, the approximation $B = B_0 + B_2 z^2$ can be made. From now on we will only take the B_0 and B_2 terms into account. The deviation from the homogeneous magnetic field can be written [Ver03] as

$$\Delta \vec{B}(\rho, z) = B_2 \left[-z\rho \cdot \vec{u}_\rho + \left(z^2 - \frac{\rho^2}{2} \right) \vec{u}_z \right] \qquad (2.21)$$

The potential energy of a magnetic dipole moment μ in an external magnetic field is $-\vec{\mu} \cdot \vec{B}$. The total potential energy of the ion, assuming a perfect quadrupolar electrical potential, is then given by

$$E_{total} = E_{el} + E_{mag} = \frac{1}{2} m \omega_{z0}^2 z^2 - \mu_z B_z \qquad (2.22)$$

where ω_{z0} is the axial frequency arising from the unperturbed quadrupolar electric field. Then the axial frequency of an ion in an inhomogeneous magnetic field can be expressed as

$$\omega_z = \sqrt{\frac{1}{m} \frac{\partial^2 E_{pot}}{\partial z^2}} = \sqrt{\omega_{z0}^2 - \frac{2}{m} \mu_z B_2^z} \approx \omega_{z0} - \frac{1}{m \omega_{z0}} \mu_z B_2^z \qquad (2.23)$$

if the inhomogeneity is small and the symmetries are kept in order to be able to express the axial component of the magnetic field as $B_z(z) = B_0^z + B_2^z z^2$.
The magnetic dipole moment of the ion μ has two components, the spin $\vec{S}$ and the orbital angular momentum $\vec{L}$. From eq. 2.23 a change in the orientation of the spin's axial projection as well as in the orbital angular momentum L, which is proportional to the energy of the reduced cyclotron motion, can be determined measuring a shift in the axial frequency $\Delta \omega_z$.

2.3 Motion of a single ion in a real trap

Due to the effects explained in the sections 2.1.2 and 2.2 the motions are not harmonic oscillators and their frequencies depend on the amplitudes (energies) of the motions. From the non-perfect quadrupolar electric potential is possible to deduce

not only a dependence of the axial frequency on the axial energy (eq. 2.14) but also an equivalent relationship for the other degrees of freedom. The same approach can be used also for the influence of the magnetic field inhomogeneity. Then, in first order approximation in a perturbative approach [Bro86], the energy dependence of the motions' frequencies can be written in the form of a matrix (including the dependence of the Larmor frequency)

$$\begin{pmatrix} \Delta\omega_+/\omega_+ \\ \Delta\omega_z/\omega_z \\ \Delta\omega_- /\omega_- \\ \Delta\omega_L/\omega_L \end{pmatrix} = M_k \begin{pmatrix} E_+ \\ E_z \\ E_- \end{pmatrix} \tag{2.24}$$

where the Matrix M_k takes different forms depending on the effect taken into account. For the electric potential anharmonicities, explained in sec. 2.1.2, the matrix takes the form:

$$M_E = \frac{6C_4}{qU_0C_2} \begin{pmatrix} +\frac{1}{4}(\omega_z/\omega_+)^4 & -\frac{1}{2}(\omega_z/\omega_+)^2 & -(\omega_z/\omega_+)^2 \\ -\frac{1}{2}(\omega_z/\omega_+)^2 & \frac{1}{4} & 1 \\ -(\omega_z/\omega_+)^2 & 1 & 1 \\ 0 & 0 & 0 \end{pmatrix}. \tag{2.25}$$

For the term corresponding to the magnetic field inhomogeneity given in eq. 2.21 the matrix can be written[2] as

$$M_B = \frac{1}{m\omega_z^2}\frac{B_2}{B_0} \begin{pmatrix} -(\omega_z/\omega_+)^2 & 1 & 2 \\ 1 & 0 & -1 \\ 2 & -1 & -2 \\ -(\omega_z/\omega_+)^2 & 1 & 2 \end{pmatrix}. \tag{2.26}$$

Combining the equations 2.24, 2.25 and 2.26 it is possible to extract the energy in the reduced cyclotron degree of freedom in units of the shift in the axial frequency $\Delta\omega_z$:

$$E_+ = m\omega_z\frac{B_0}{B_2}\Delta\omega_z. \tag{2.27}$$

Finally relativistic corrections have to be taken into account. Keeping in mind the relation between the frequencies $\omega_- \ll \omega_z \ll \omega_+$, one gets in the classical approximation the matrix

$$M_R = \frac{-1}{mc^2} \begin{pmatrix} 1 & 1/2 & -(\omega_z/\omega_+)^2 \\ 1/2 & 3/8 & -\frac{1}{4}(\omega_z/\omega_+)^2 \\ -(\omega_z/\omega_+)^2 & -\frac{1}{4}(\omega_z/\omega_+)^2 & \frac{1}{4}(\omega_z/\omega_+)^4 \\ 2/9 & 1/2 & -(\omega_z/\omega_+)^2 \end{pmatrix}. \tag{2.28}$$

2.4   Detection of ions

In order to be able to measure the electronic *g-factor* we have to be able to observe quantum jumps in the spin degree of freedom. This is only possible with the suited accuracy, if performed on a single ion. Thus, it is necessary to implement a detection system capable of detecting single ions. For this purpose an electronic scheme was chosen [Deh68, Win75, Sta98, Häf98]. It relies on the fact that the object to be

---

[2]For getting this simple expression the approximation $\omega_+ \simeq \omega_c$ is done. A more precise calculation can be found in [Her96] and [Her99]
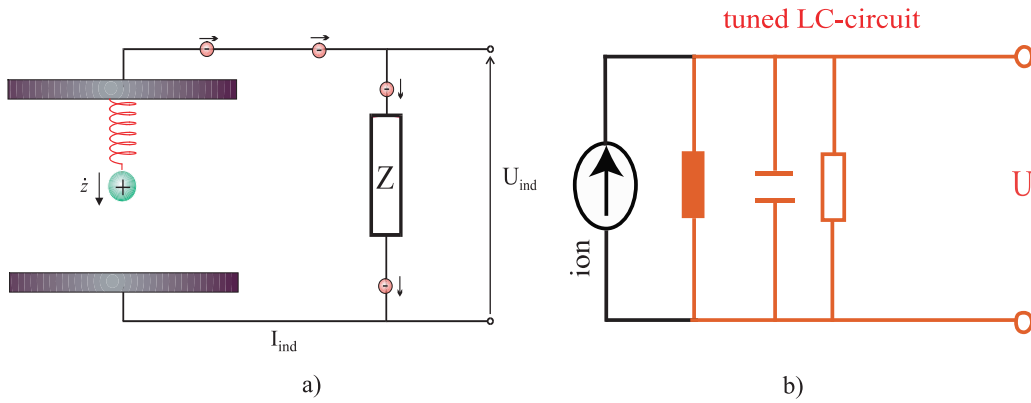
Figure 2.6: **Model of the electronic detection. a) Spring model on which the electronic detection is based. b) First approximation to the equivalent circuit of the combination of a tuned LCR-circuit and an ion.**

detected is a charged particle which oscillates harmonically between two conducting surfaces, the trap electrodes. Then as the charged particle, in our case a hydrogen-like ion, approaches one of the electrodes it induces some charge on its surface. By closing a circuit with an impedance (fig. 2.6a) between the two electrodes which correspond to the opposite phases of the motion, it is possible, in principle, to measure an AC current flowing through the impedance. Since the motion of the ion is an harmonic oscillator its frequency is well-defined and therefore the frequency of the AC current induced by the ion will coincide with the frequency of the ion itself. Of course this current is very small since it is induced by only one ion. It is actually measured as a potential difference in the ends of the impedance. The impedance conformed by an LC-circuit (fig. 2.6b) is tuned at the ion's frequency. In order to analyze the current flowing through the circuit it is interesting to calculate the ion's equivalent circuit [Sta98].

2.4.1 Ion's equivalent circuit

We will now discuss the interaction of an ion with the surrounding electronics. To simplify the problem we will try to deduce the equivalent circuit of an ion confined in a Penning trap oscillating in the z-direction[3]. We will use a simple model [Win75] in which the motion of the ion is produced by an electrically neutral and massless spring with spring constant $k = m\omega_z{}^2$ where m is the ion's mass and ω_z its axial frequency in the trap. The recovering force that the ion feels, if moved from its equilibrium, can be written as

$$F = -k \cdot z. \tag{2.29}$$

We now add an extra AC potential difference $U(t)$ applied to the endcaps. Then a

---

[3]For simplicity, we discuss the detection of the axial motion, from the results given, the calculations for detection in the radial plane are straight-forward.

time-dependent electrical field

$$E_z(t) = \frac{U(t)}{2z_0} \qquad (2.30)$$

is created. In eq. 2.30 the approximation of a planar capacitor (instead of the hyperbolical shape of the classical Penning trap electrodes, see fig. 2.7) was taken in order to simplify the calculations. $2z_0$ is the separation between the capacitor's electrodes which coincides with the separation between the endcaps.
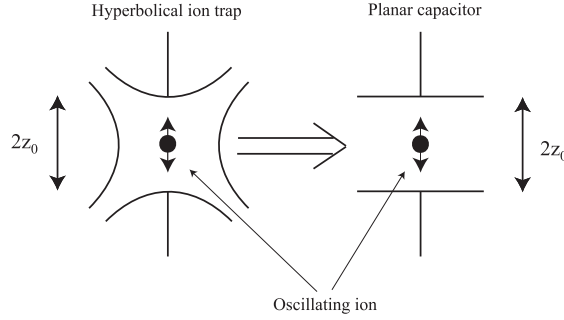

Figure 2.7: **Approximation of an hyperbolical trap to a capacitor of infinitely big planar electrodes with an electrode separation $2z_0$, coinciding with the electrode separation in the hyperbolical trap.**

For a more precise description it is possible to introduce a correction factor γ which accounts for the curvature of the real electrodes and their finite size [Win75] and changes the inter-electrode distance $2z_0$ to an effective distance $d_{eff} = 2\gamma z_0$.
From the electric field the ion gets an additional periodic drive in the direction of the z-axis

$$F_{AC}(t) = q \cdot E_z(t) = \frac{qU(t)}{d_{eff}}. \qquad (2.31)$$

The equations of motion can be now written as

$$m\ddot{z} = F + F_{AC}(t) = -m\omega_z^2 \cdot z + \frac{qU(t)}{d_{eff}}. \qquad (2.32)$$

On the other hand, the oscillation of the ion represents an alternating current between the endcap electrodes of magnitude

$$I = q\frac{\dot{z}}{d_{eff}}. \qquad (2.33)$$

From this expression it is possible to rewrite the equation of motion substituting the current I by the axial coordinate z. This gives

$$U = m\frac{d_{eff}^2}{q^2}\Big(\dot{I} + \omega_z^2 \int I dt\Big). \qquad (2.34)$$

Equation 2.34 can be simplified by defining the constants

$$l_i = m\frac{d_{eff}^2}{q^2} \qquad (2.35a)$$

$$c_i = \frac{1}{l_i\omega_z^2} \qquad (2.35b)$$

which yield

$$U = l_i \cdot \dot{I} + \frac{1}{c_i} \int I dt. \tag{2.36}$$

Equation 2.36 relates the voltage on the ends of a series resonant LC-circuit with the current which flows through it. The deviation of the electric field created at the center of the trap from the one created by the planar electrodes of the capacitor qU/d_{eff} must be taken into account. Therefore, we introduce a constant α which modifies the ion's inductance to $l_i = m\frac{d_{eff}^2}{\alpha q^2}$. By coupling inductively this circuit to
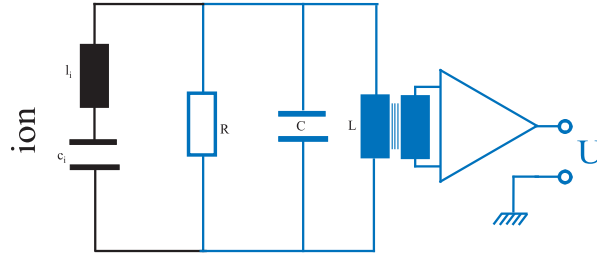
Figure 2.8: **Complete equivalent circuit of the ion and the tuned LCR-circuit coupled with an external amplifier which allows the electronic detection of ions in a Penning trap.**

an external amplifier (fig. 2.8), it is possible to measure the combined noise spectrum of the ion's lc-circuit in parallel with the tuned resonant LCR circuit. The result of combining the two resonant circuits will give a Lorentz line shape for the LCR tuned circuit that is shortcut at the resonance frequency of the lc ion's equivalent circuit. This can be seen for three different cases in fig. 2.9.
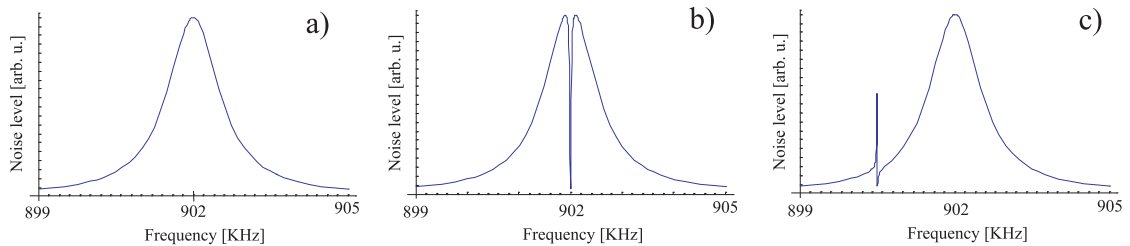
Figure 2.9: **Theoretical noise spectrum of the tank circuit: a) without ion, b) with an ion oscillation's frequency in the center of the resonance, c) with an ion oscillation's frequency far detuned**

This can be generalized to an ion cloud formed by N ions of the same species. It is possible to obtain the ion number by use of this equivalent circuit. Let us assume that the center of mass corresponds to the center of charge, and that an ion's cloud center of mass behaves in an ion trap in the same way as a single ion with charge $q_c = Nq$ and mass $m_c = Nm$ (where q and m are the charge and mass of the single ion). Then, it is possible to calculate the resonance of the equivalent circuit of the cloud. The inductance of the cloud l_c is given by

$$l_c = \frac{m_c d_{eff}^2}{q_c^2} = \frac{Nm d_{eff}^2}{(Nq)^2} = l_i/N. \tag{2.37}$$

On the other hand, the resistance R of the lc-circuit at resonance can be obtained from

$$R = \frac{\omega_{res} l_c}{Q} \tag{2.38}$$

where Q is the quality factor of the resonant circuit given by $Q = \omega_{res}/\Delta\omega$. Then, from 2.37 and 2.38 one gets

$$N = \Delta\omega \frac{l_i}{R} = \Delta\omega \frac{m d_{eff}^2}{q^2 R} \tag{2.39}$$

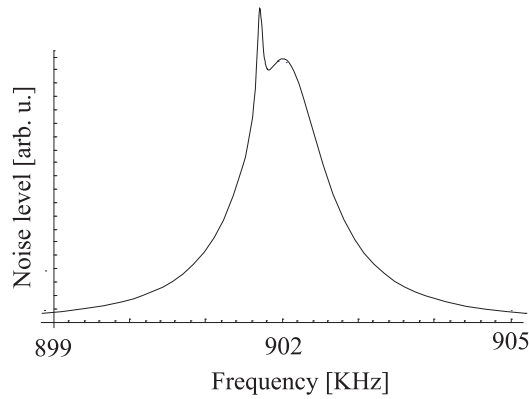which makes it possible to determine the ion number from the width of the ions' dip.

Figure 2.10: **Calculated noise spectrum of the tank circuit with an ion cloud slightly detuned.**

The model presented above for the detection of ions is valid only for the case of ions and tank circuit in thermal equilibrium. But for the case of "hot" ions it is easier to explain the detection in terms of the voltage increase in the terminals of the LC-circuit produced by the ions while they dissipate their energy through the cold electronic circuit. In this case, instead of a dip in the Johnson-noise of the tank circuit, a peak superimposed to it is observed (fig. 2.10). This way of detecting ions is proven to be much faster because no thermal equilibrium is needed and the signal to noise ratio can be controlled simply by exciting the ions' motion. In contrast the frequency measurements arising from this kind of detection are less accurate due to the fact that the frequencies of the motions may depend on the motions' energies if the electric potential is not harmonic or the magnetic field is not homogeneous.

2.5   Line-shape of the Larmor resonance

Good knowledge of the line-shape of the Larmor resonance is necessary in order to estimate all possible contributions to the systematical uncertainties in the determination of the electronic g-factor. In this section the Larmor resonance will be discussed. The so-called Larmor frequency, $\omega_L = g\frac{\mu_B}{\hbar}B$, is the precession frequency of the spin around an external magnetic field B. It also corresponds to the energy of the Zeeman splitting induced by the same magnetic field B.

The so-called Rabi formula (deduced in many text books, e.g. [Sak85, All87])

$$P(t) = \frac{\Omega^2}{\Omega^2 + \left(\frac{\omega_{MW} - \omega_0}{2}\right)^2} \sin^2 \left[\left(\Omega^2 + \left(\frac{\omega_{MW} - \omega_0}{2} \right)^2 \right)^{\frac{1}{2}} \cdot t \right] \qquad (2.40)$$

gives the probability of inducing a quantum jump, $\Delta E = \hbar \omega_0$, between the levels of an atomic two level system in presence of an electromagnetic wave of frequency ω_{MW} and a magnetic field amplitude B_{MW} in a time t. In eq. 2.40 $\Omega = \frac{e\hbar}{m_e} B_{MW}/\hbar$ is the so-called Rabi frequency at resonance. Taking into account that our irradiation time is very long (of the order of minutes) the term in $\sin^2$ can be replaced by its average $(1/2)$. This, for the case of an electron spin with an applied microwave signal at a frequency near the Larmor frequency ω_L, gives

$$P(t) = \frac{1}{2} \frac{\Omega^2}{\Omega^2 + \left(\frac{\omega_{MW} - \omega_0}{2}\right)^2} \qquad (2.41)$$

that is a lorentzian line-shape with a maximum amplitude of $1/2$ for the probability of inducing an quantum jump between the two spin states, so called spin-flip.

But in the case of an electron bound in a hydrogen-like ion which is confined in a Penning trap (see sec. 2.1) with an inhomogeneous external magnetic field the Larmor frequency depends on the path of the ion in the trap. Therefore, it depends on the energies of all degrees of freedom (E_+, E_- and E_z for the reduced cyclotron, magnetron and axial motion respectively). Thus, the line-shape 2.41 has to be modified according to all these dependencies.

An extensive study was done by J. Verdú [Ver03] and J. Verdú *et al.* [Ver04] obtaining a probability for inducing a quantum-jump when irradiating with a microwave of frequency ν_{MW} given by:

$$P(\nu_{MW}; E_+, E_z) = \frac{1}{2} \frac{\left(\frac{B_{MW}}{2\pi^2 B_0}\right)^2}{\left(\frac{B_{MW}}{2\pi^2 B_0}\right)^2 + \left(g_0 + \alpha_+ E_+ + \alpha_z E_Z - \frac{\hbar \omega_{MW}}{\mu_B B_0}\right)} \qquad (2.42)$$

where g_0 is the theoretical g-factor (see table 1.1) and α_+ and α_z are, respectively, coefficients derived from the energy dependence of both the reduced cyclotron and the axial frequency. They are given by:

$$\alpha_+ = -\frac{B_2}{B_0} \frac{g_0}{m\omega_+^2} \left[1 + \frac{\omega_+}{2\omega} \frac{B_1^2}{B_0 B_2} \left(1 - \frac{\omega_z^2}{2\omega_+^2} \right) \right] \qquad (2.43)$$

$$\alpha_z = \frac{B_2}{B_0} \frac{g_0}{2m\omega_+ \omega}. \qquad (2.44)$$

From these equations, resonance curves can be plotted to try to understand the behavior and shape of the Larmor resonance as a function of several parameters such as cyclotron energy, axial energy or amplitude of the applied microwaves in order to optimize the measurement process to avoid possible systematical errors.

As can be seen in figures 2.11 and 2.12, the main effect of the cyclotron energy on the Larmor resonance is an overall linear shift of the resonance. From equations 2.24, 2.25 and 2.26 it can be seen that the cyclotron energy can be given in units of an axial frequency shift through the relation $E_+ \approx 2.0852\pi \Delta\omega_z$.

In figures 2.13 and 2.14 the dependence of the Larmor resonance with the axial energy is shown. The energy is given in terms of the associated temperature [Dje04]. In the plot in fig. 2.13 it can be observed that a higher axial temperature leads not only to a shift in the center frequency and a broadening of the resonance but also to a decrease of the maximum spin-flip probability. This effect makes it important to control the axial temperature and to try to bring it to the lowest possible value, since a lower axial energy would not only decrease systematic uncertainties but also
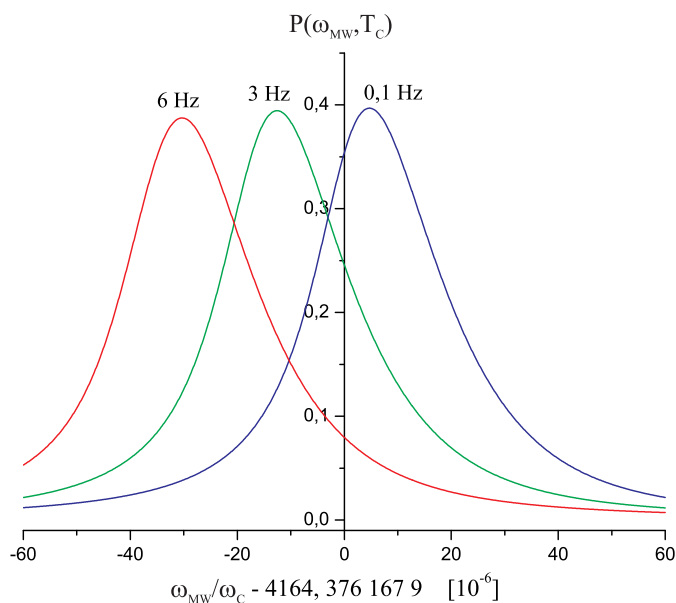
Figure 2.11: **Plot of the Larmor resonance as a function of the cyclotron energy. The energy is expressed in terms of the shift in the axial frequency.**
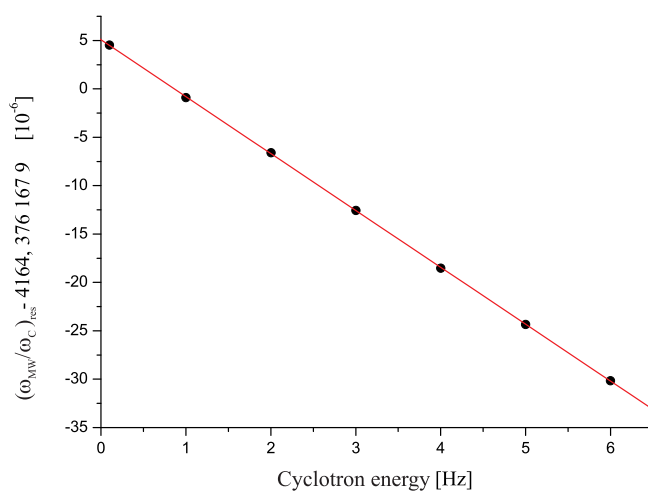
Figure 2.12: **Plot of the center of the Larmor resonance. The energy is expressed in terms of the shift in the axial frequency.**

would increase the spin-flip probability and thus decrease the measurement time.

Figures 2.15 and 2.16 show the behavior of the spin-flip probability while varying the power of the irradiated microwaves. This power is given in fig. 2.15 as the amplitude of the magnetic field associated to the irradiated microwaves. In fig. 2.16 the power is given as the spin-flip probability at the maximum of the resonance, which is the accessible quantity in our measurements.

In all these figures (2.14-2.16) the resonances are given in terms of the ratio ω_{MW}/ω_C
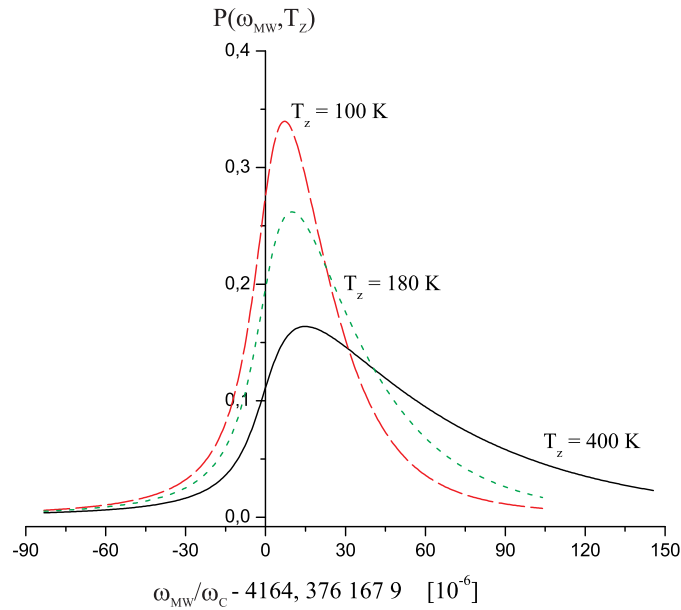
Figure 2.13: **Plot of the Larmor resonance as a function of the axial energy. The energy is given in terms of the temperature. The cyclotron energy is negligible and the microwave amplitude is such that $B_{MW} \approx 7$ mG.**
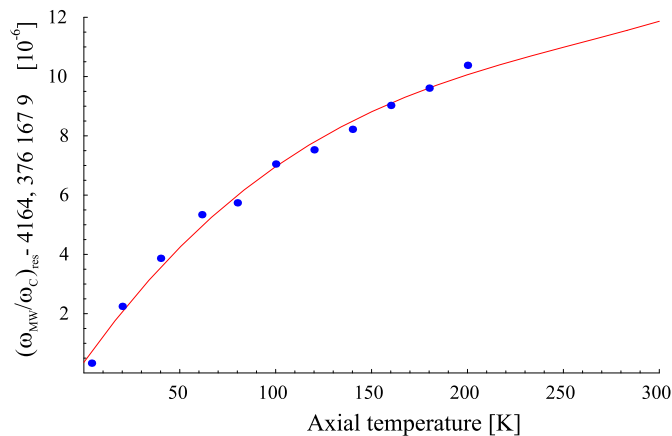
Figure 2.14: **Plot of the center or the resonance as a function of the axial energy. The solid line represent the least-squares fit to a third order polynomial.**

between the applied microwave frequency ω_{MW} and the measured cyclotron frequency ω_C in order to simplify the comparison with the experiment.
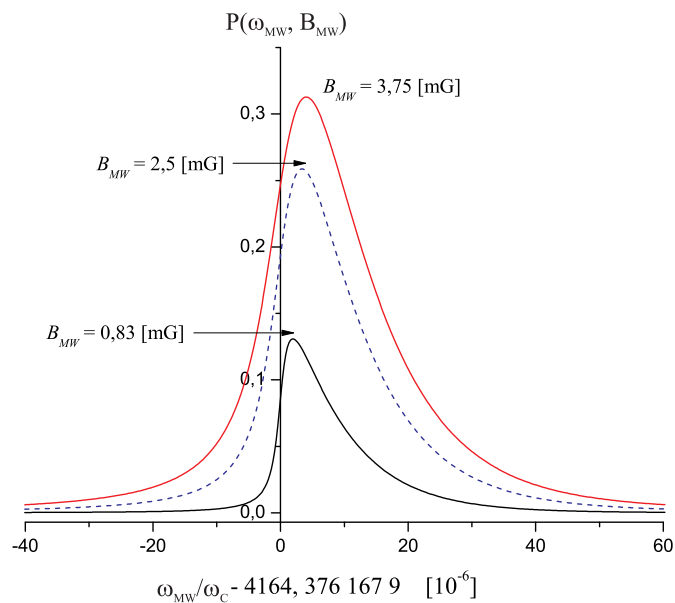
Figure 2.15: **Plot of the Larmor resonance as a function of the applied microwave power. The power is given by the magnetic field amplitude of the microwaves. The cyclotron energy is negligible and the axial temperature is set to be $T_z = 61$ K in all curves.**
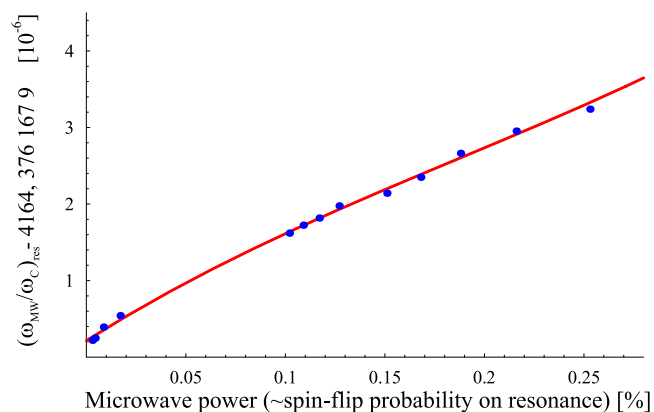
Figure 2.16: **Plot of the center or the resonance as a function of the applied microwave power. The power is given in terms of the spin-flip probability in the maximum of the resonance in the lower plot.**

Chapter 3

Experimental setup and method

> An expert is a person who has made
> all the mistakes that can be made in
> a very narrow field.
>
> Niels Bohr

The Mainz Stern-Gerlach setup was planned as a first step on the way towards bound-state QED tests on highly charged ions up to U^{91+}. It was built by Stefan Stahl, Nikolaus Hermanspahn and Manfred Tönges. A detailed description can be found on the doctoral thesis of Stefan Stahl [Sta98]. The first test and measurements were performed mainly by Nikolaus Hermanspahn [Her96, Her99] and Hartmut Häffner [Häf98, Häf00]. In this chapter an overview of the experimental setup and the measurement procedure will be given.

3.1 Setup

The core of the experimental apparatus is a cylindrical Penning trap which is located in the evacuated bore of a superconducting magnet. The complete setup (see fig. 3.1) includes:

- superconducting magnet and its cryostat, including the liquid helium and nitrogen dewars

- trap's vacuum chamber

- cryogenic electronics

- liquid helium and nitrogen dewar for the apparatus

- room temperature electronics

The magnet is running a field of 3.8 T with an homogeneity on the order of 10μ T/mm^2 at the location of the ion trap. The ion trap is actually composed of two independent trapping regions, the so-called analysis and precision traps. Both of them are composed by a stack of five electrodes (see fig. 3.2): two endcaps, two correction electrodes and a ring. In the case of the analysis trap the ring is made of a ferromagnetic material (Nickel) to create a quadratic inhomogeneity of the magnetic field of about 10 mT/mm^2 in order to be sensitive to the spin direction of the ion (see section 2.2).

The trap is enclosed in a sealed vacuum chamber at liquid helium temperature. Due to the cryopumping effect the pressure is below 10 $^{-16}$ hPa [Her99]. This upper limit for the pressure was obtained from the estimation of the free main path of the ion which was calculated from the measurement of the storage time of ion cloud of $^{12}C^{5+}$.
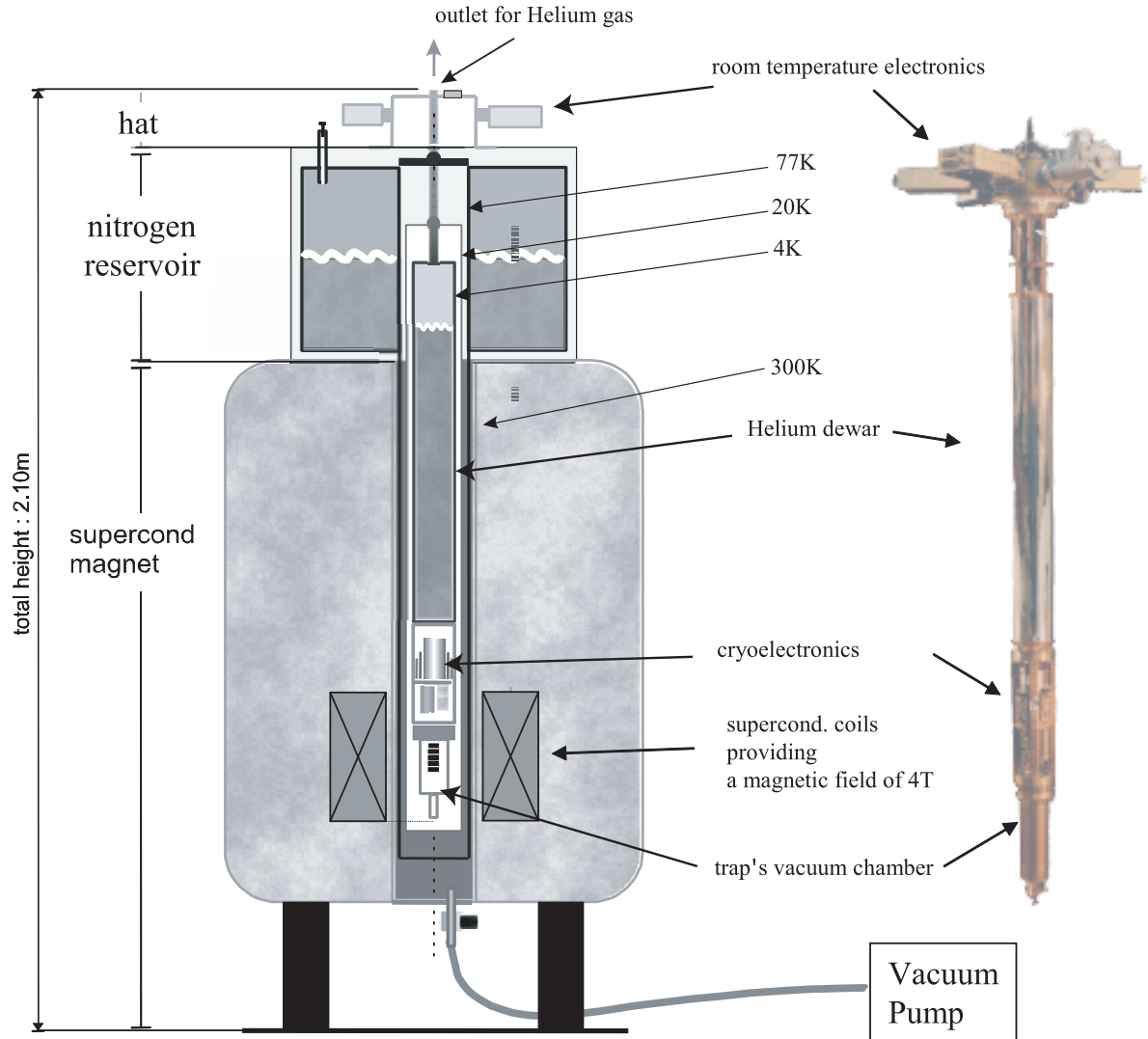

Figure 3.1: **Overview of the magnet and the apparatus. The apparatus (right) where the most important parts of the setup are located. There are the trap's vacuum chamber, the cryoelectronics which allow the detection of a single ion and the helium dewar cooling the apparatus to 4.2 K.**

Just above the trap's vacuum chamber sit the cryogenic electronics, composed by three LC-circuits and the corresponding amplifiers. These electronics are in the 4.2 K region in order to be able to reduce the noise temperature of the amplifiers and to make possible the implementation of superconducting resonators. For more details see sections 2.4 and 3.1.4.

On top of the cryoelectronic region the liquid helium reservoir is located. Is is in charge of maintaining the trap and the electronics at 4.2 K. It is shielded from the external world through an electropolished aluminium tube which is in thermal contact with the helium vapor, at roughly 20 K. This completes the cold insert sitting in the evacuated bore of the magnet whose walls are in contact with an extra liquid nitrogen reservoir. On top of the insert is located the so-called *hat*.

In order to induce quantum jumps in the spin degree of freedom (spin-flips) in a 3.8 Tesla field a 105 GHz microwave signal is needed. The solution chosen in the present setup is to use a six times multiplied 17.5 GHz signal coming from a commercial microwave generator. This is achieved by feeding the 17.5 GHz signal in a two-step ($2x$ and $3x$) frequency multiplier which contains a GaAs based ISIS-varactor diode. The diode is built in a high quality resonator so that the outgoing signal is only the 6 times multiplied one, yielding an optimized spectral purity. Then, the microwaves are guided in the apparatus through a hollow wave guide, which is interrupted in the *hat* and at the entrance to the trap vacuum chamber in order to preserve the two different vacuum levels. At this points a teflon and a quartz window, respectively, are placed. For more information on the microwave system see [Im98, Tön96].

3.1.1 Room temperature electronics

In the room temperature region there are two different parts, the *hat* electronics and the control and data acquisition electronics. The *hat* is the part of the setup sitting in the top of the cryostat. There are six feedthroughs connecting the "outer world" with the traps and the 4 K-electronics. A set of electronic devices whose task is to care about the purity of the signals going in and out of the 4 K region is located there. In addition to that, in the room temperature region one can find many electronic devices which deal with the control of the whole experiment and also with the data acquisition. As an example one can mention: several function generators ranging from DC up to 20 GHz; a microwave 6-fold multiplier in order to get the 105 Ghz corresponding (approximately) to the electron's Larmor frequency in a field of 3.8 Tesla; two realtime-FFT[1]-analyzers; a precision voltage source; an 80 channel precision multimeter; and the electronics that control the voltages in the trap and in the cryo-amplifiers. The control of the signals and voltages and the data acquisition and pre-analysis are performed by a Pascal-based programm running on an average PC. The programm was first programmed by Stefan Stahl and further developed by all the other students working in the experiment.

3.1.2 Magnet

To produce the suitable magnetic field of 3.8 T we make use of a commercial magnet. The magnet it self is build of a NbTi solenoid which is superconductive at liquid helium temperature. It is able to produce a magnetic field strength up to 6T. It is built in a special configuration with a 12cm diameter bore to make it possible to introduce the traps' vacuum chamber, the cryoelectronic setup and the cryostat for cooling them. The bore is evacuated at a pressure of about 10 [7] hPa in order to produce the thermal insulation needed for the inserted cryostat.
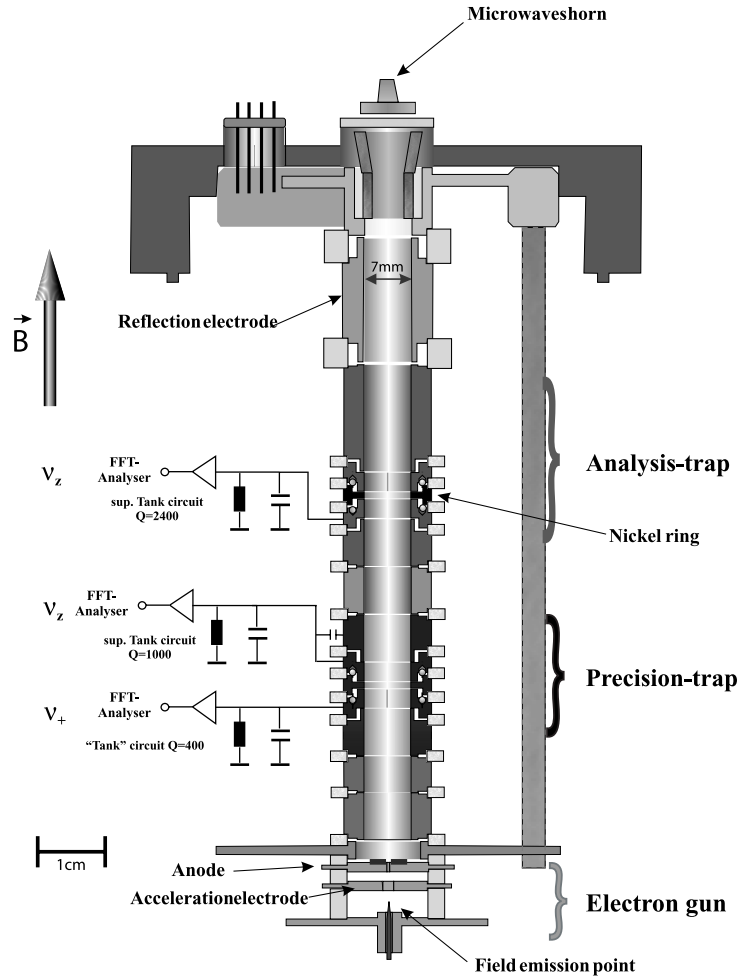
---

[1]Fast Fourier Transform

Figure 3.2: **Electrode stack. Indicated are the two different trapping regions, the attached detection electronics and the electron gun with its components**

3.1.3   Cryostat

In addition to the magnet's cryostat, our setup includes a second cryostat which cares for the low temperature electronics and helps to produce the vacuum needed in the trapping region in order to get the needed storage time for achieving the suited accuracy. This second cryostat is composed of three concentric cylinders sitting inside the bore of the magnet. The inner one is actually a cylindrical container, made of copper and is filled with 5 liters of liquid helium. In order to minimize thermal losses there is a second cylinder made of electropolished aluminium. This second cylinder is cooled by the evaporating helium vapor at a typical temperature of roughly 30 K [Her96]. The outer one is kept at 77 K due to its thermal contact with the inner surface of the bore of a cylindric dewar that is built on top of the magnet to contain an extra amount of liquid nitrogen (in fig. 3.1 labelled nitrogen reservoir).
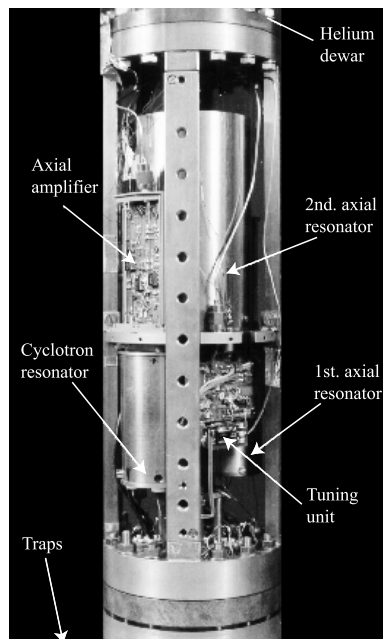
Figure 3.3: **4 Kelvin electronics region. Shown are the three resonators, one of the amplifiers and the GaAs-switch for tuning the cyclotron LC-circuit**

3.1.4   Cryoelectronics

The main tool for detecting single ions is the cryoelectronics setup. This part of the setup is composed by three LC resonant circuits and the three corresponding preamplifiers (fig. 3.3). The LC-circuits are composed of a coil in a metallic housing and the main contribution to the capacitance is due to the parasitic capacitances of both the wiring and the trap electrodes. The circuits can be classified into two types due to the different frequency ranges that they are supposed to deal with. In one hand the ones used to detect the axial motion of the ions (in the range of 300-1000 KHz) and the one used for detecting the modified cyclotron motion, in the range of 25 MHz. The axial resonators are composed of a coil made of a niobium-titanium alloy, which is superconducting at 4.2 K (for the mentioned frequency range), enclosed in a NbTi housing. The inductances of such coils are 1.2 mH and 4.7 mH for the precision and the analysis trap, respectively. The quality factors are around 1000 and 2500 at resonance frequencies of 920 KHz and 370 KHz for the precision and the analysis trap, respectively, at 4.2 K. And in the other hand the one used for the reduced cyclotron frequency a copper (non-superconducting) coil is used since at that frequency range (25 MHz) the difference in the quality factor from normal copper to the superconducting NbTi alloy is small. Another factor is that the difficulties connecting the superconducting material to the normal conductors do not pay when compared with the small improvement in the quality factor of the resonant circuit. The circuit for reduced cyclotron motions has an extra set of switchable capacities which implements the possibility of decoupling the ion from the detection circuit.

3.1.5   Double Penning trap

In the present experiment a double trap setup is used in order to be able to spatially separate the two main tasks: the determination of the spin state (analysis of the spin direction) and the induction of changes on this degree of freedom, spin-flips, while measuring the frequencies of the motions. The double trap arrangement is shown in figure 3.2. The name of the traps (analysis and precision) are given by the main function of each trap. Both traps are geometrically alike, and as described in section 2.1.2 with the dimensions given in table 2.1. The only difference between the two traps is the fact that the ring electrode of the analysis trap is made of a NiFe alloy, which is ferromagnetic, in order to produce the magnetic field inhomogeneity needed for the observation of the spin state.

3.1.6   Ion production

The goal of the present experiment is to study highly charged ions. The ions can be created outside and then introduced in the trap. This solution is not used in our case because it would make difficult and expensive to achieve the suited conditions of pressure and temperature in the trap. However, as it is done in this case, the ions can created inside the trap through a process similar to the one used in electron beam ion traps (EBITs). For this purpose, as is shown in fig. 3.4, the trap has in the lower end a field emission point (FEP) which if connected to a high negative voltage will emit electrons in the direction of the so-called acceleration electrode. The acceleration electrode is at a positive voltage, and the voltage difference between the FEP and the acceleration electrode determines the electron current. Once the electrons are emitted from the FEP they are "trapped" by the high magnetic field and they must follow the magnetic field lines where they were emitted. They fly in towards the other end of the trap where they encounter the rejection of the so-called reflection electrode, which is at a high negative voltage (around 100 V more negative than the FEP). Thus, they must come back along the same way they arrived. Electrons from the FEP are continuously added to the beam, and the coulomb repulsion between the electrons increases the beam radius. After a while some of the electrons collide with the edges of the anode, where the carbon target is located. The electrons extract some atoms from the target's surface. These atoms diffuse all around the target. Some of them receive further electron impacts with enough energy to ionize them. These ions get caught in the potential minimum that is set for this purpose in the precision trap, where they can be further ionized, step wise, by the still flowing electron beam. From this procedure one obtains an ion distribution of many species in many ionization stated (see figure 3.5).

Monitoring of the production process

Once ions are created a typical procedure is to monitor the contents of the trap. This is performed with the help of mass spectra. The procedure to obtain a mass spectrum relies on the fact that the axial frequency of the ions is a function of the ring potential and of their charge-to-mass ratio, $\omega_z^2 \propto q/m \cdot V$. Then if an LC-circuit with resonant frequency ω_0 is connected to the trap's correction electrodes and the ring potential is ramped between V_1 and V_2, all ions with a value for the mass-to-charge ratio in the interval $[V_1/\omega_0, V_2/\omega_0]$ will get in resonance successively
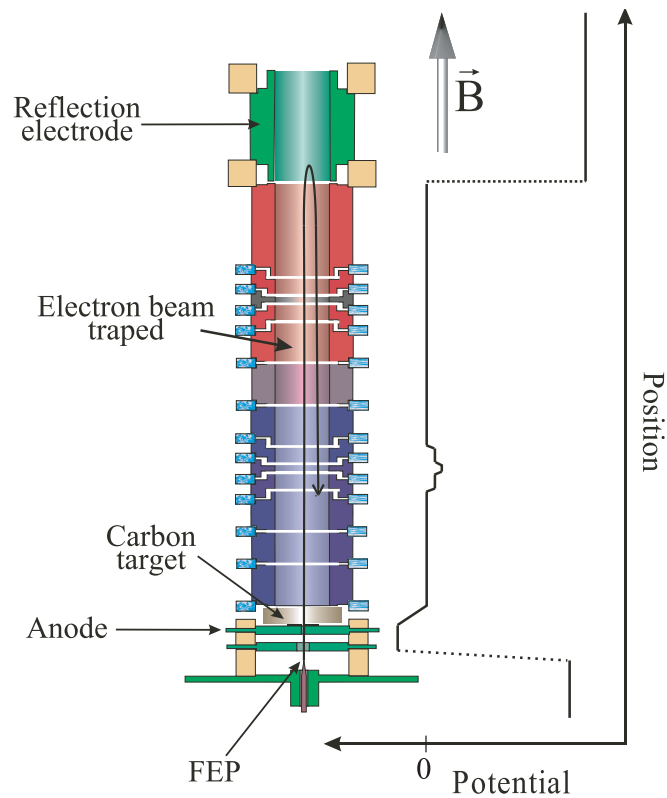
Figure 3.4: **Scheme of the double Penning trap. On the bottom a diagram of the potential levels of the trap's different regions during the ion creation is shown. The dark arrow is a representation of the electron's beam path.**
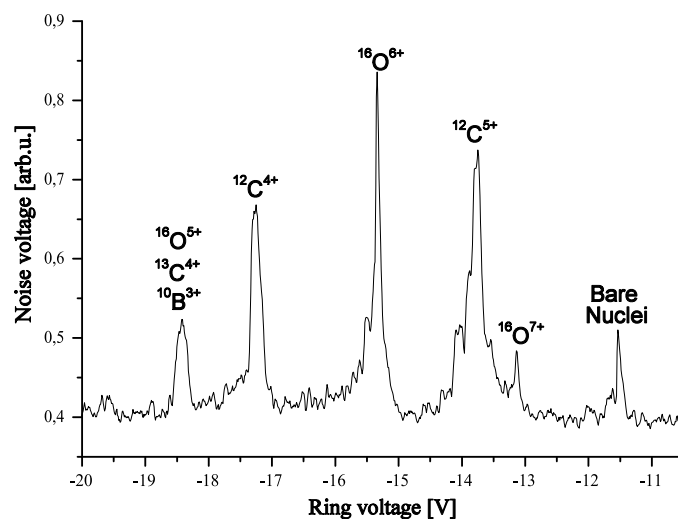

Figure 3.5: **Example of a mass spectrum after creation of an ion cloud. Observable are peaks corresponding to carbon and oxygen in different ionization states, and possibly other atomic species. The different ring voltages correspond to different charge-to-mass ratios.**

with the resonant circuit if the ring voltage is such that for this species the relation $\omega_0 = \omega_z(q/m)$ is fulfilled. Then, if the ions are hot, an increase in the noise voltage in the terminals of the LC-circuit is observable. Thus, picking out this voltage increase and plotting it against the ring voltage it is possible to monitor the contents of the trap (see fig. 3.5).
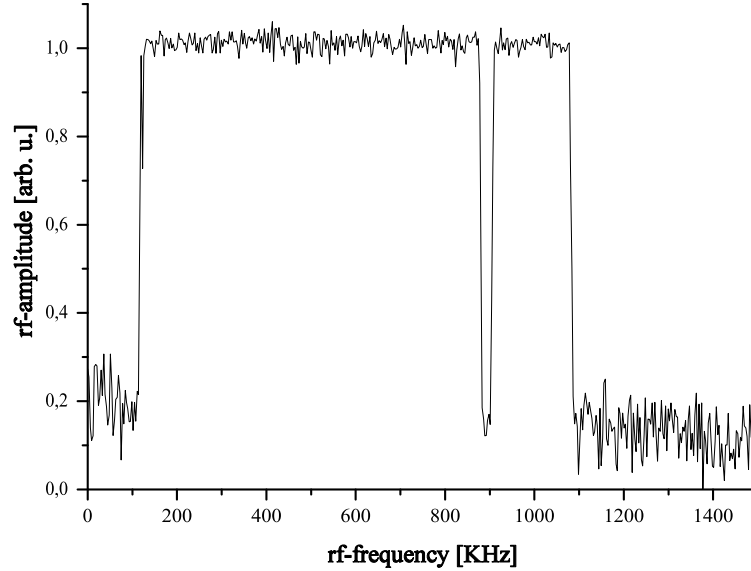
Figure 3.6: **Noise spectrum of the signal used for selectively exciting all the ion species but the one of interest for the experiment. In this case the species with axial frequency around 900 KHz are not excited, i.e. $^{12}C^{5+}$ for a ring voltage of -13.2 V.**

Purification of the ion cloud

After this first detection of the trap's contents, the next step is to try to get a pure cloud of one specific ion species. In order to achieve this goal, the procedure used in our experiment is to perform a cycle of exciting the unwanted ions and lowering the potential well hoping to kick out only the unwanted ions. This excitation is done by irradiation of a rf-signal which consists of noise in all frequencies but in the axial one of the ion of interest (see figure 3.6). After several applications of the cycle of excitation and lowering the potential well. A mass spectrum yields a result similar to the one in figure 3.7.

3.2 Single ion preparation and measurement of mode frequencies

Once a pure cloud of the desired ion species is isolated in the trap, it is possible to go further in the process of isolating a single ion. In order to monitor this part of the process the techniques for single ion detection and frequency measurement are needed. Here these techniques will be presented. At the same time the process toward a single ion will be discussed.
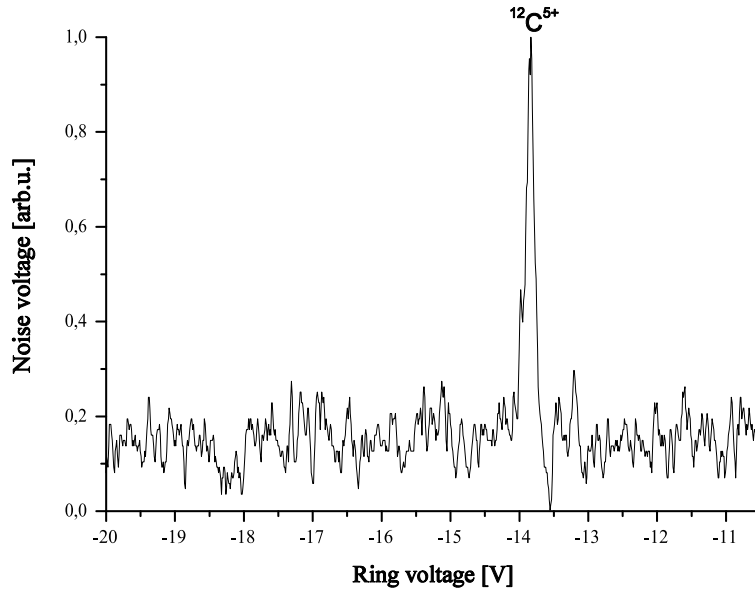
Figure 3.7: **Example of a mass spectrum after several purifying cycles. The peak corresponding to $^{12}C^{5+}$ is visible.**

3.2.1   Ion counting and the reduced cyclotron frequency

The first thing to do is to count the number of ions in the cloud. There are two possible ways. One relies on the fact, as explained in sec. 2.4.1, that the width of the dip produced by a small ion cloud while short-cutting the Johnson-noise of the LC-circuit is proportional to the number of ions in the cloud. For counting the ions they should be in thermal equilibrium with the tank circuit, which is not necessarily the case in the process of ion creation. Another technique makes use of the fact that, even in the most homogeneous region, the magnetic field is not perfectly homogeneous and the cyclotron frequency (and therefore the reduced cyclotron frequency) depends on the radius of the cyclotron orbit. This implies that the reduced cyclotron frequency depends on the energy of this degree of freedom. Since in an ion sample, like a cloud, the ions' cyclotron energy follows a statistical distribution their cyclotron frequencies will follow the same distribution [Dje04]. Then if the noise spectrum is observed in detail, it is possible to distinguish several peaks, one for each ion, on the top of the Johnson-noise of the tank circuit (sec. 2.4.1, fig. 3.8). At this point is possible to further proceed with the process to leave one single ion. The next step is to excite the ions cyclotron motion and to lower, very carefully, the well potential. If done carefully enough, a single ion is lost, and then it is possible to proceed until one single ion is left in the trap. Once a single ion appears in the noise spectrum (fig. 3.9) it is possible to measure its reduced cyclotron frequency with an accuracy on the order of 10^{10}. The next step is to try to observe the ion's signal in thermal equilibrium with the tank circuits.

3.2.2   Cooling of the motional modes

As explained in section 2.3, the frequencies depend on the energy in each motional mode. Thus, to avoid any systematic error they should be measured at the smallest
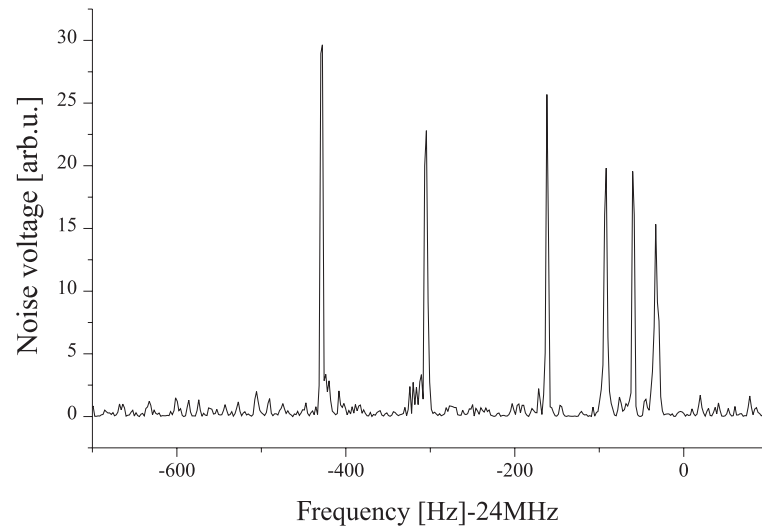
Figure 3.8: **FFT analysis of the noise on the LC-circuit attached to the split correction electrode in the precision trap. It shows the peak of 6 $^{12}C^{5+}$ ions.**
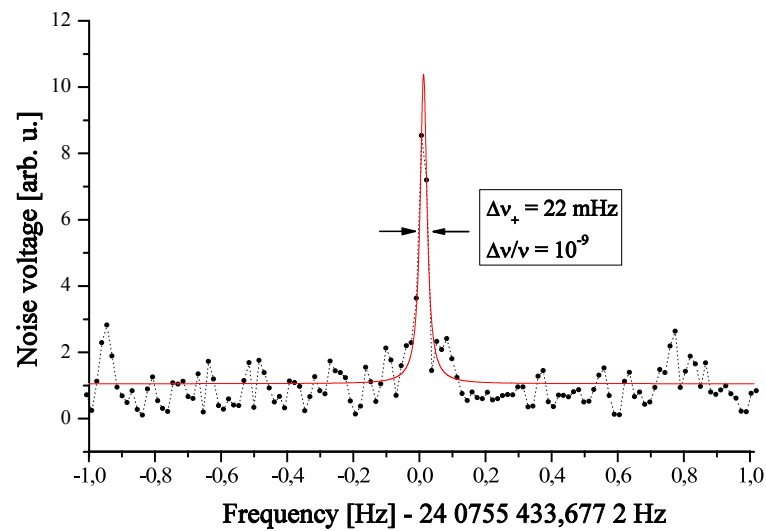

Figure 3.9: **A single $^{12}C^{5+}$ ion signal observed in the FFT analysis of the noise on the cyclotron LC-circuit in the precision trap.**

possible energies. Like all physical systems left on their own, the ion will reach the thermal equilibrium with its environment after certain a time. In this system, the liquid helium acts as an infinite thermal bath, so the ion at some point will reach the "temperature" of 4.2 K [Dje04]. The dissipation of the energy of the ion takes mainly place due to the ohmic part of the LC-circuits, which is why this kind of cooling is called resistive cooling. Actually, equations 2.32 and 2.33 represent a damped harmonic oscillator where the damping of the ion motion is introduced by the tank circuit. The damping constant is then

$$\gamma = \frac{q^2}{4mz_0^2}R \tag{3.1}$$

where R is the real part of the total impedance Z of the resonant circuit. Actually, if measured as a function of time, the reduced cyclotron frequency shows (fig.3.10) the characteristic exponential dependency of the resistive cooling with a time constant of about 4 minutes.
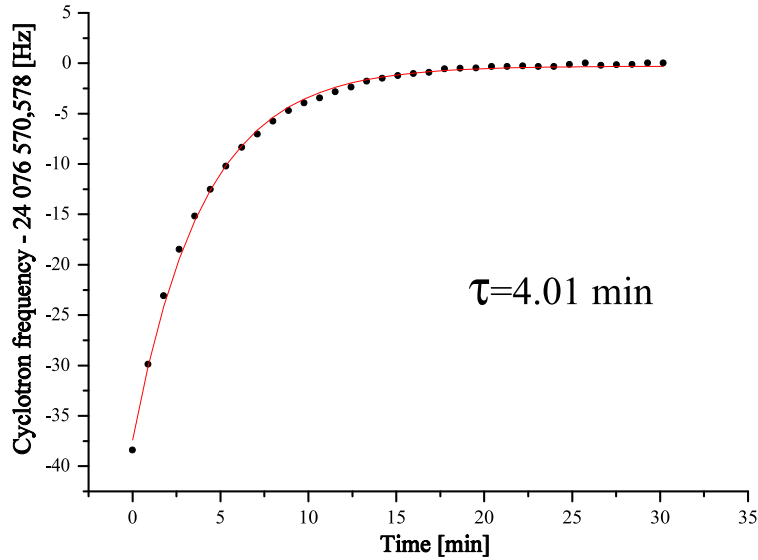
Figure 3.10: **Cyclotron Resistive cooling. A time constant of 4.01 minutes is observed. The exponential behavior of the frequency in time results from dependency of the reduced cyclotron frequency with the energy in this degree of freedom due to the residual magnetic field inhomogeneity.**

3.2.3 Axial motion

Once the ion is in thermal equilibrium with the resonant circuits, it is possible to observe its signal in the noise spectrum of the tank circuit as a shortcut in the Johnson-noise of the circuit (sec. 2.4.1). In a Penning trap the magnetron motion cannot be coupled to any LC-circuit since the magnetron radius increases as energy is dissipated (eq. 2.11). The motions that are coupled to the resonant circuits (axial and reduced cyclotron motion) can be detected with the technique explained in sec. 2.4. The frequency of the motions can be obtained from the FFT analysis of the voltage on the LC-circuits. The width of the resonance $\Delta\omega$ of a single ion depends
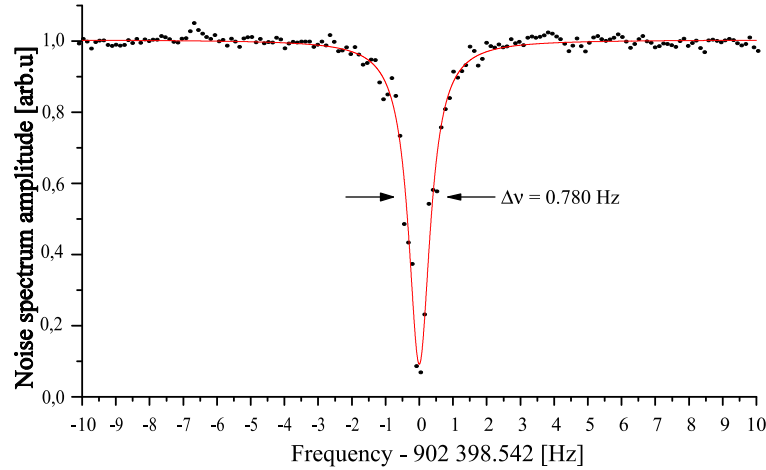
Figure 3.11: **FFT analysis of the noise voltage on the LC-circuit connected to the upper endcap of the precision trap showing the axial dip. From the width of 780 mHz a cooling time constant of 203 ms is obtained.**

(eq. 2.39) on the resonance resistance of the LC-circuit and, thus, on the quality factor. This width can be predicted from the cooling time constant τ of the motion since from eq. 2.39 and eq. 3.1 one gets $\tau = 1/\gamma = 1/\Delta\omega$. The reduced cyclotron motion's signal cannot be observed directly as a dip in the noise spectrum of the tank circuit because, due to the high frequency of this motion, it is challenging to obtain quality factors high enough. In the case of our experiment, with a cooling time constant for the reduced cyclotron motion of around 4 minutes, the expected width is about 0.6 mHz@25 MHz. That is beyond the accuracy of any available spectrum analyzer. Due to the lower frequency domain, the axial motion is much more favorable for this detection scheme. Indeed, the quality factors of the axial tank circuits in both traps ($Q \simeq 1000$ and $Q \simeq 1500$ in the precision and the analysis trap, respectively) provide much bigger damping than in the case of the reduced cyclotron motion, which implies a much wider dip. This dip (fig. 3.11) is about 0.8 Hz@1 MHz and 2 Hz@370 KHz in the precision and the analysis trap, respectively. From these widths it is possible to estimate the cooling time constants for the ion's axial motion, which are in the range of 50 to 200 ms.

In some cases, it is desirable to obtain an axial signal as fast as possible. In these cases the signal/noise ratio is improved by artificially increasing the Johnson-noise level of the tank circuit. Since the ion's signal shortcuts the Johnson-noise if its level is higher, then the dip would be also bigger and thus easier to observe. This increase in the Johnson-noise level is produced applying an r.f.-signal that is set to be squared in frequency domain (see fig. 3.12). This technique is also used to control the harmonicity of the trap by monitoring the frequency shift of the ion comparing the axial frequency with and without the square signal on the tank circuit.

Optimizing the tuning ratio

The tuning ratio was defined in section 2.1.2 as the ratio between the voltages applied to the ring and the correction electrode. If the potential well is not perfectly harmonic
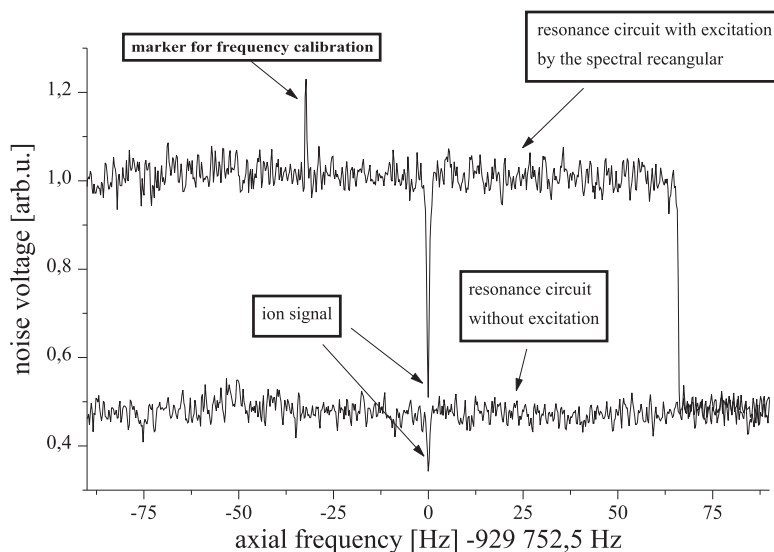
Figure 3.12: **Axial signal on the FFT analyzer with and without increase of the Johnson noise level. An improvement of the signal/noise ration is easy to appreciate.**
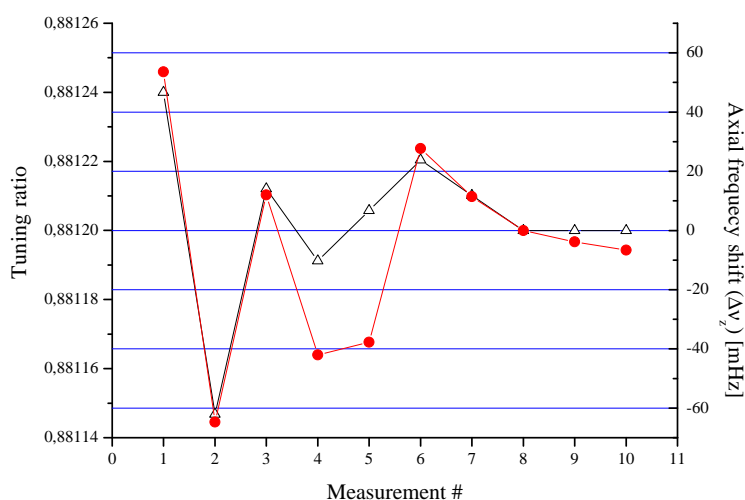

Figure 3.13: **Tuning ratio optimization. Circles represent the axial frequency shift and the open triangles the applied tuning ratio.**

the axial frequency depends on the energy of the ion this fact is used to optimize the tuning ratio, thus, to make the potential well as harmonic as possible. This is done by measuring the axial frequency of the ion at several axial energies and studying the dependence of the frequency shift with the applied tuning ratio. The axial energy is controlled by increasing the tank circuit Johnson-noise level as described above. The optimization if performed in an automatic mode. The procedure is as follows: a

tuning ratio is set, the axial frequency is measured, a square signal is applied to the tank circuit (fig.3.12) and the axial frequency is measured again. Then the tuning ratio is changed according with the value of the frequency shift, if the shift is positive the tuning ratio is decreased and the other way around. This procedure continues until the frequency shift is smaller than a set value, typically 10mHz, that makes it acceptable for the precision measurements. In figure 3.13 the frequency shift is plotted together with the applied tuning ratio.
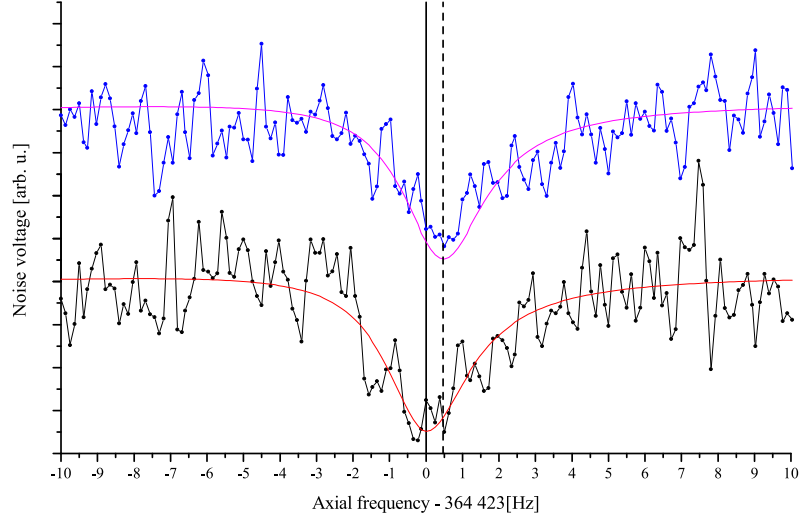
Figure 3.14: **Axial signals for the two different possible orientations of the ion's spin. A shift of about 0.6Hz can be observed.**

3.3   Detection of Spin-flips

In order to measure the electronic *g-factor* we make use of the fact that the Zeeman energy level splitting of an atomic ion in a magnetic field B is given by:

$$\Delta E_{zeeman} = \hbar\omega_L \tag{3.2}$$

where ω_L is the Larmor precession frequency of the ion's spin around the magnetic field and can be expressed as:

$$\omega_L = g\frac{e}{2m_e}B \tag{3.3}$$

e being the positive elementary charge and m_e the electron's mass. The magnetic field at the ion's position can be determined by a measurement of the ion's true cyclotron frequency

$$\omega_C = \frac{q}{m_i}B \tag{3.4}$$

where q/m_i is the ion's charge-to-mass ratio. Then combining eq. 3.3 and eq. 3.4 one gets

$$g = 2\frac{\omega_L}{\omega_C}\frac{q}{e}\frac{m_e}{m_i} \tag{3.5}$$
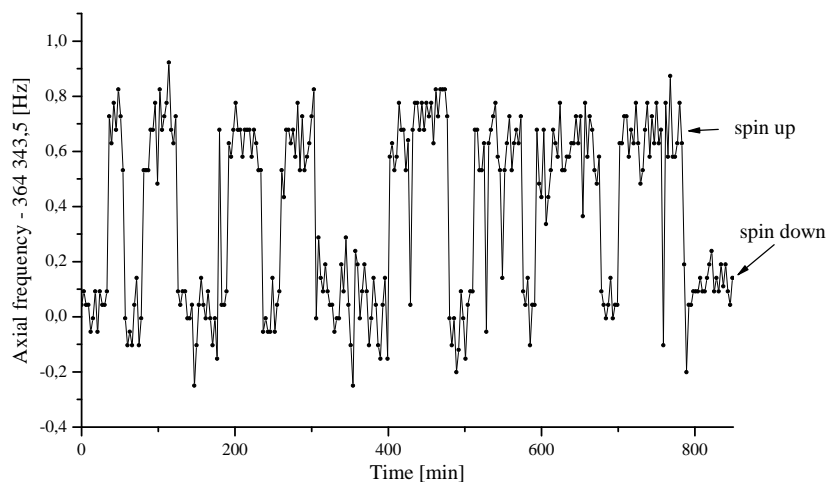
Figure 3.15: **Ion's axial frequency in the analysis trap, plotted as a function of time while microwaves are irradiated quasi-resonantly with the Larmor frequency. It can be observed that the 0.6Hz frequency jump while a spin-flip occurs is much bigger than the average fluctuations of the axial frequency.**
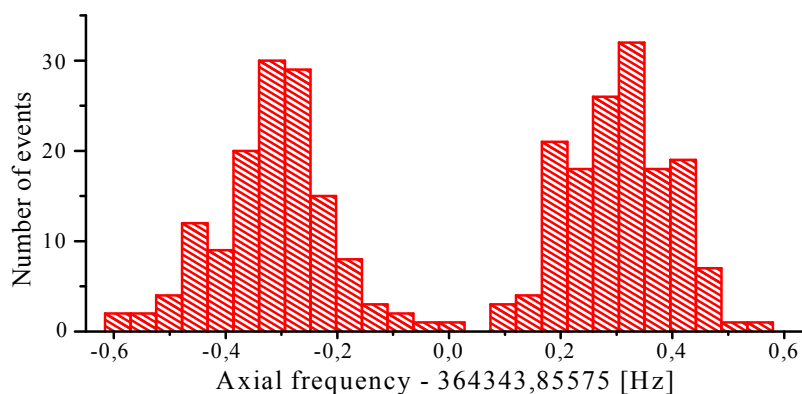
Figure 3.16: **Histogram of the frequencies in the fig. 3.15. The distinct two level distribution of the frequency points shows the possibility of distinguishing both spin states.**

Thus, a simultaneous measurement of the Larmor precession frequency and cyclotron frequency gives a way to determining the ion's *g-factor*. In case of an ion with with vanishing angular momentum, e.g. an ion with an even-even nucleus, the ion's

g_J-*factor* coincides with the electronic *g-factor*. As shown above with the present
setup is possible to determine the cyclotron frequency within an uncertainty in the
order of 10 ^{10}. Now a way of determining the Larmor frequency will be discussed.
The spin is an internal degree of freedom but making use of an inhomogeneous
magnetic field O. Stern and W. Gerlach shown that it can be coupled to the motion
of the particle. In fact a modification of the Stern-Gerlach experiment was proposed
by H. Dehmelt to perform a quantum non-demolition experiment in which the spin
orientation relative to a magnetic field can be determined by observing the axial
frequency of a charged particle in confined in a Penning trap. This is the so called
continuous Stern-Gerlach effect [Deh86]. This effect relies on the fact that the axial
frequency of a charged particle in an inhomogeneous magnetic field depends on its
magnetic moment (eq. 2.23). In fact for our setup the frequency jump corresponding
to a quantum jump in the spin degree of freedom is:

$$|\Delta\nu_z(\text{spin-flip})| = \frac{g \ \mu_B \ B_2}{4\pi^2 \ m_{ion} \ \nu_{z0}} \approx 0.65 \text{ Hz} \qquad (3.6)$$

where $\nu_{z0} \approx 365$ kHz is the unperturbed[2] axial frequency in the analysis trap where
the magnetic field is inhomogeneous due to the nickel ring-electrode. Since the ac-
curacy in the measurement of the axial frequency is better than 500 mHz (fig. 3.11)
it is possible to determine the spin orientation by comparing measurements of the
axial frequency (fig. 3.14). This is also possible because the frequency jump is bigger
than the fluctuations on the axial frequency (fig. 3.15 and fig. 3.16).

---

[2]The unperturbed axial frequency is the axial frequency of the ion in Penning trap with a
perfectly homogeneous magnetic field.

Chapter 4

Results

4.1   Motional mode coupling

As explained in section 3.2.1, the frequency of the reduced cyclotron motion cannot be measured if the motion is in thermal equilibrium with the resonant circuit because the dip produced by the ion while shortcutting the Johnson-noise of the LC-circuit is too narrow for being detected. This and the dependence of the modified cyclotron frequency on the energy imposes a limit in the accuracy in our measurements. To overcome this problem a new method for measuring the frequencies that are not accessible directly was developed. This new method relies on the fact that if two harmonic oscillators are coupled then the resulting motion is amplitude modulated. In this section the behavior of the axial motion while coupled with the other two motions, the perturbed cyclotron and the magnetron motion, will be discussed.

As a first approach, the coupling of the cyclotron an the axial motion will be described. For this coupling an r.f.-signal of a frequency $\omega_\gamma = \omega_+ - \omega_z + \delta$ is introduced, where δ is a small detuning. This r.f.-field is applied to one part of a split correction electrode thus the field has quadrupolar geometry. Let the driving field be

$$E_\gamma = \mathcal{E}_\gamma e^{i\omega_\gamma t}(z\hat{u}_x + x\hat{u}_z) \tag{4.1}$$

where $\mathcal{E}_\gamma$ is the amplitude of the driving field. Then taking the cyclotron motion as a one-dimensional harmonic oscillator along the x axis, the equations of motion are now

$$\ddot{z} + z\,\omega_z^2 = \frac{q}{m}Re\left[\mathcal{E}_\gamma e^{i\omega_\gamma t}\right]x \tag{4.2a}$$

$$\ddot{x} + x\,\omega_+^2 = -\frac{q}{m}Re\left[\mathcal{E}_\gamma e^{i\omega_\gamma t}\right]z. \tag{4.2b}$$

A possible solution for this equation of motion is then

$$z = \frac{Re\left[Z(t)e^{i\omega_z t}\right]}{\sqrt{\pi m \omega_z}} \tag{4.3a}$$

$$x = \frac{Re\left[X(t)e^{i\omega_+ t}\right]}{\sqrt{\pi m \omega_+}} \tag{4.3b}$$

where $Z(t)$ and $X(t)$ are slowly varying functions of time. With the definition

$$\Omega = \frac{iq\mathcal{E}_\gamma}{2m\sqrt{\omega_z\omega_+}} \tag{4.4}$$

which gives a measurement of the coupling strength in frequency units, the solutions take the form

$$\dot{Z} = \frac{\Omega}{2}e^{-i\delta t}X \tag{4.5a}$$
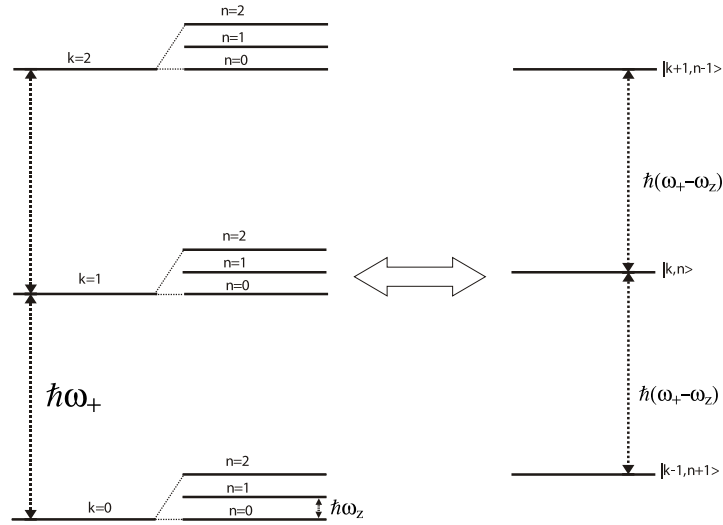
$$\dot{X} = \frac{-\Omega}{2}e^{+i\delta t}Z. \tag{4.5b}$$

Figure 4.1: **The two harmonic oscillators are equivalent to a single oscillator of frequency $\omega_0 = \omega_+ - \omega_z$. For the analogy with the dressed-atom only the transition $|k,n\rangle \leftrightarrow |k-1,n+1\rangle$ will be taken into account.**

Then one can distinguish 2 cases:

- $\delta = 0 \Longleftrightarrow$ Resonant coupling

  While coupling is on we have

$$Z(t) = \frac{\Omega}{|\Omega|}X_0 \sin\left(\frac{|\Omega|t}{2}\right) + Z_0 \cos\left(\frac{|\Omega|t}{2}\right) \tag{4.6a}$$

$$X(t) = -\frac{\Omega}{|\Omega|}Z_0 \sin\left(\frac{|\Omega|t}{2}\right) + X_0 \cos\left(\frac{|\Omega|t}{2}\right) \tag{4.6b}$$

  where Z_0 and X_0 are the initial condition for the functions $Z(t)$ and $X(t)$ and are complex numbers proportional to the initial phase and action of the axial and reduced cyclotron motion. In this case, the effect of the coupling is that the motion oscillates between a pure axial motion and a pure radial motion. If

the pulse has the strength and duration t such that $|\Omega| \cdot t = \pi$ then after the pulse

$$Z(t) = \frac{\Omega}{|\Omega|} X_0 \qquad (4.7a)$$

$$X(t) = \frac{-\Omega}{|\Omega|} Z_0. \qquad (4.7b)$$

which means a complete exchange of the amplitudes on x and z direction.
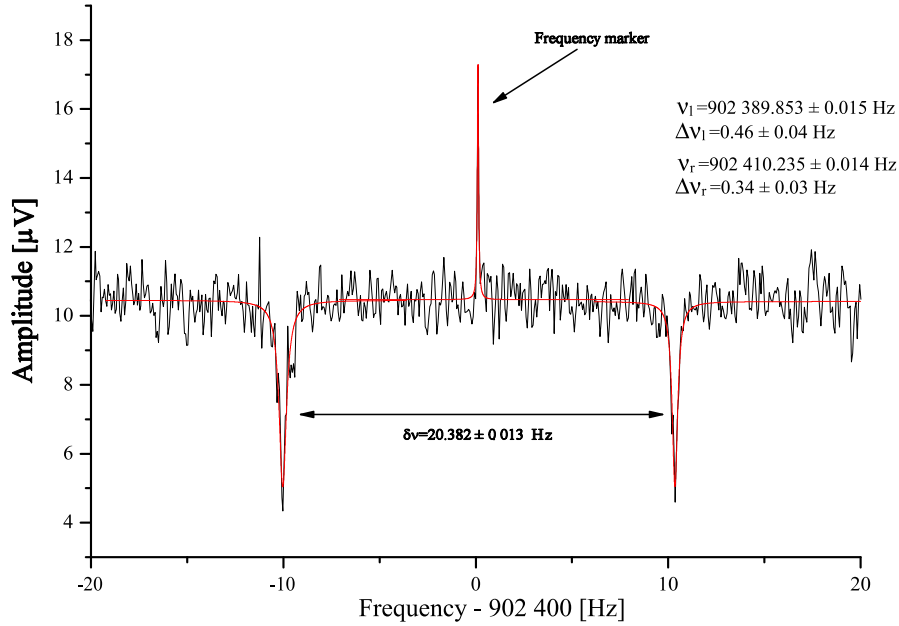
Figure 4.2: **FFT analysis of the noise spectrum in the region of the axial mode. This spectrum was taken while simultaneously a quasi-resonant coupling rf-signal was applied. The two side dips are the two components of the split axial mode. The central peak is a frequency marker generated by a atomic clock locked frequency generator in order to evaluate possible shifts of the internal clock of the spectrum analyzer. The solid lines are lorentzian fits to the peak and dips.**

- $\delta \neq 0 \iff$ non-resonant coupling and classical avoided crossing

This case is easier to study by analogy with the dressed-atom approach [Dal85]. The problem of the coupling of the two motions by the electromagnetic field is analogous to the problem of a forced quantum harmonic oscillator of frequency $\nu_0 = \nu_+ - \nu_z$ (fig. 4.1) and the driving force has the frequency $\nu_\gamma = \nu_0 + \delta$. By analogy with a driven oscillator it is expected that the resulting oscillation has a frequency which differs from the original one by ν_γ. With the ion oscillating in the axial direction at a frequency $\nu = \nu_z + \epsilon$ with $\epsilon \ll \omega_z$ and in the reduced cyclotron motion at $\nu + \nu_\gamma = \nu_+ + \epsilon + \delta$ an ansatz could take the form

$$Z(t) = C_z e^{i\epsilon t} \tag{4.8a}$$

$$X(t) = C_x e^{i(\epsilon + \delta)t}. \tag{4.8b}$$

With these solutions for the functions $Z(t)$ and $X(t)$, substituting in eq. 4.5a one gets the following expression for ϵ

$$\epsilon = \frac{-\delta}{2} \pm \frac{1}{2}\sqrt{\delta^2 + |\Omega|^2} \tag{4.9}$$

which means that each one of the coupled modes of the motions split into two modes with a difference in frequency of $\nu_r - \nu_l = \epsilon_+ - \epsilon_- = \sqrt{\delta^2 + |\Omega|^2}$, which depends both on the detuning of the coupling frequency and on the strength of the coupling. With the same kind of arguments, it is possible to get an analogous solution for the coupling between the axial an the magnetron motion.
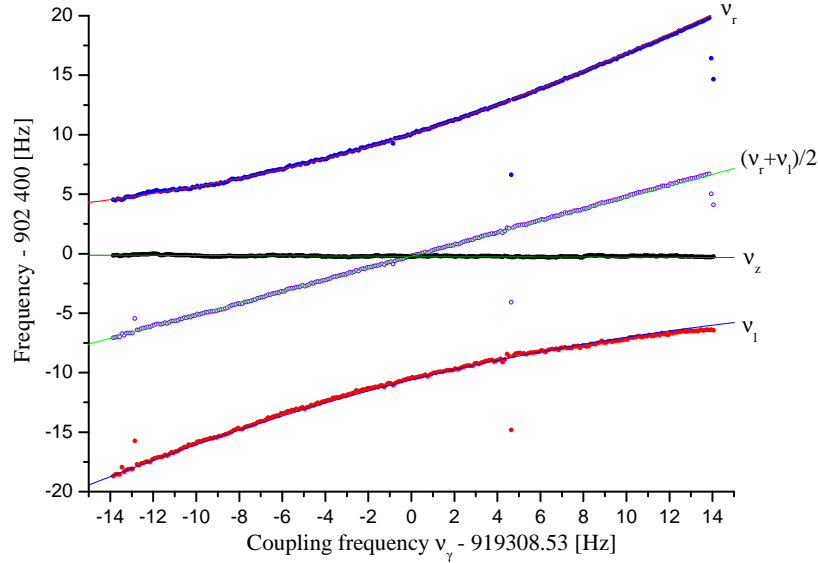
Figure 4.3: **Mode frequency as a function of the coupling frequency detuning for the coupling of the axial with the magnetron motion. Solid lines represent least-square-fits of the data. The horizontal data points are the measured axial frequencies that drift 130 mHz during the the measuring time of 1200 minutes for the left plot and 80 mHz during the 480 min. for the right one. The diagonal data points corresponds to the average value of the two modes' frequencies which equals the axial frequency for resonant coupling, i.e. vanishing detuning. And finally the other two data set are the split modes' frequencies.**

4.1.1 Mode splitting

As discussed in the previous section, if coupled the motional the modes split into two. Thus, a spectrum with two dips can be observed. An example of such a spectrum is shown in figure 4.2 where a frequency window of 40 Hz span in the region of the axial mode is taken while a quasi-resonant coupling is applied. Now lets analyze the behavior of the "new" modes as a function of the parameters of the coupling, namely the detuning and the strength.
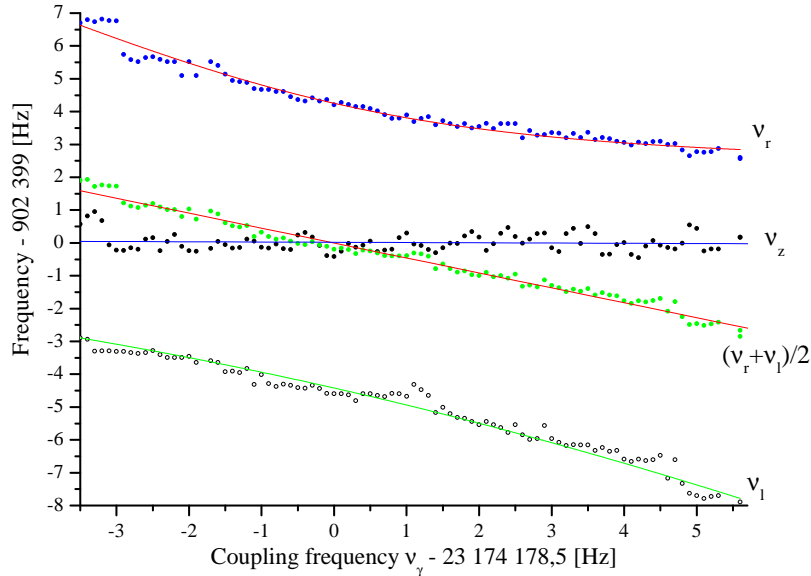
Figure 4.4: **Mode frequency as a function of the coupling frequency detuning for the coupling of the axial with the cyclotron motion. Solid lines represent least-square-fits of the data to** $\nu_r, l = \nu_z - \frac{\delta}{2} \pm \frac{1}{2}\sqrt{\delta^2 + |\Omega|^2}$ **for the two split modes and to** $\nu = a + b\delta$ **for the axial and average frequencies.** δ **is the independent variable in both cases.**

In figure 4.3 and in figure 4.4 the behavior of the modes as a function of the coupling frequency is plotted both for the coupling of the axial mode with the magnetron and the cyclotron motion, respectively. This represents the picture of the so-called classical avoided crossing [Cor90]. From the fits in this kind of plot it is possible to extract both the coupling strength and a value for the resonant frequency. These two parameters can also be extracted from plots where the mode separation is presented against the detuning δ. In figure 4.5, the solid line denotes the fit to $\sqrt{\delta^2 + |\Omega|^2}$, where δ is the independent variable. From the minimum mode separation it is possible to extract the strength of the coupling. In fig. 4.6, of the mode separation vs. the amplitude of the applied r.f-signal, which is proportional to the strength of the coupling (eq. 4.4), the solid line is the fit to $\sqrt{\delta^2 + (\alpha|V|)^2}$, where the independent variable is set to be $V = \Omega/\alpha$. The detuning δ is in this case set to be 3.4 Hz. The proportionality constant α between the Ω and the applied signal amplitude V, was obtained from the same kind of fit for different values of the detuning and is found

to be $\alpha = 40.5 \pm 0.2$. This is consistent with the value obtained from the comparison of the measured strength, from the plot of the separation vs. detuning (fig. 4.5, with the amplitude of the applied signal, that was $V_{pp} = 0.5$V.
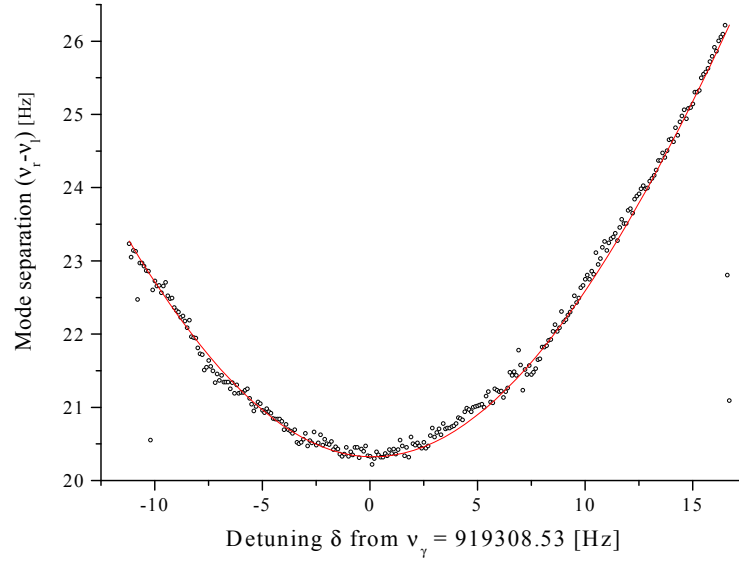

Figure 4.5: **Mode separation as a function of the detuning for a fixed coupling strength. The solid line is a least-squares fit to $\sqrt{(\delta - \delta_0)^2 + |\Omega|^2}$ were $\delta_0 = 0.14 \pm 0.07$ Hz and $|\Omega| = 20.32 \pm 0.03$ Hz**
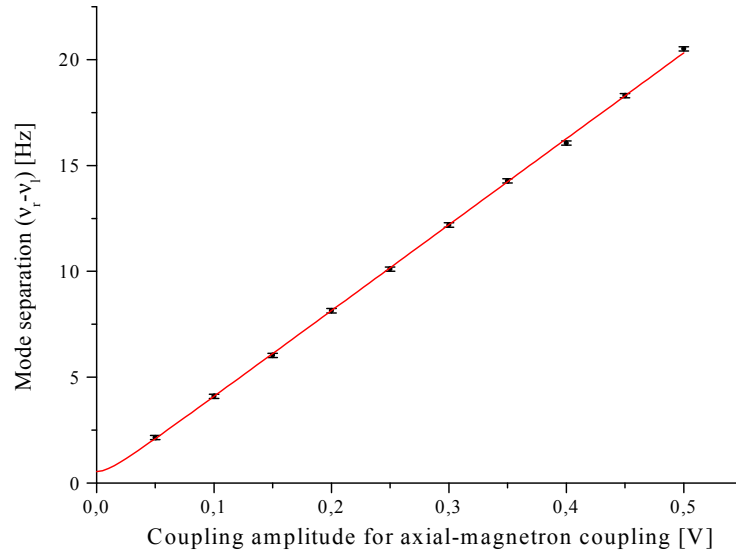

Figure 4.6: **Mode separation as a function of the coupling amplitude for a fixed value of the detuning. The coupling amplitude is given by the amplitude in V_{pp} of the applied signal at the output of the frequency generator. The solid line is a least-squares fit to $\sqrt{\delta^2 + (\alpha V)^2}$ being $\delta = 0.5 \pm 0.3$ Hz and $\alpha = 40.63 \pm 0.12$ Hz/V**

4.2 Determination of the magnetron frequency

The free cyclotron frequency of a charged particle in a Penning trap cannot be measured directly because the cyclotron is not a proper motion in the trap. In contrast, as shown in previous sections, the axial and reduced cyclotron motion can be determined with high accuracy. In order to determine the *g-factor*, the free cyclotron and not the reduced cyclotron frequency has to be measured. In the present experiment this is done by measuring all three frequencies corresponding to the three degrees of freedom. Then, according to the so called invariance theorem [Bro86]:

$$\nu_C^2 = \nu_+^2 + \nu_z^2 + \nu^2 \tag{4.10}$$

The problem is that the magnetron frequency can also not be measured directly since the motion is an harmonic oscillator with negative potential energy, i.e. the energy decreases with the increase of the amplitude of the motion. If the ion is coupled to a tank circuit the energy will flow out of the motion and thus the ion gets lost. A possible solution is to measure the magnetron frequency in an indirect way, namely by coupling the axial and the magnetron motions. Then, in a similar way as explained above, the modes split into two and now the frequencies of the split axial mode are given by:

$$\nu_{r,l} = \nu_z + \frac{\delta}{2} \pm \frac{1}{2}\sqrt{\delta^2 + |\Omega|^2} \tag{4.11}$$

From eq. 4.11, if the axial frequency is known, one can determine the detuning δ of the coupling frequency simply by adding the frequencies of the two modes

$$\delta = (\nu_r + \nu_l) - 2\nu_z \tag{4.12}$$

and then, since the coupling frequency ν_γ is a priori known, the magnetron frequency can be calculated as $\nu = \nu_\gamma - \nu_z - \delta$.

Reduced cyclotron→	$\nu_+=$	24 075 434 Hz
Axial →	$\nu_z=$	902 398 Hz
Magnetron →	$\nu =$	16 910 Hz

Table 4.1: **Frequencies of the motions in the precision trap.**

From the values of the frequencies (table 4.1) in each degree of freedom the total contribution to the uncertainty to the determination of the free cyclotron frequency from eq. 4.10 can be calculated to be:

$$\begin{aligned} \Delta\nu_C &= \frac{\nu_+}{\nu_c}\Delta\nu_+ + \frac{\nu_z}{\nu_c}\Delta\nu_z + \frac{\nu}{\nu_c}\Delta\nu \\ &\approx 0.9993\Delta\nu_+ + 0.0374\Delta\nu_z + 0.0007\Delta\nu \ . \end{aligned} \tag{4.13}$$

And thus, assuming absolute uncertainties for the direct measurements of the axial and reduced cyclotron frequencies of 0.3Hz and 25mHz respectively one get an accuracy in the free cyclotron frequency in the order of 10^{-9} provided the measurement of the magnetron frequency is accurate on the level of 30 Hz. A magnetron frequency measurement gives the typical value of $\nu = 16\,910.5 \pm 0.4$ Hz .

4.3   Method to measure the cyclotron frequency

As seen in section 3.2.1, the reduced cyclotron frequency can be measured with high accuracy through the Fourier analysis of ion's image current. But as explained there, for such a measurement the ion has to be excited since the cyclotron dip would be too narrow to be detected. As the magnetic field is never completely homogeneous, the measured cyclotron frequency depends on the ion's energy (eqs. 2.24, 2.25 and 2.26), in this degree of freedom. This dependence of the measured reduced cyclotron frequency with the ion's energy may lead to systematic errors if not corrected properly. In principle, a possible way of avoiding this error is to measure the frequency for several different energies and then extrapolate to vanishing energy. An alternative approach is to measure the reduced cyclotron energy using the same method used for the magnetron frequency, namely extract it from the coupling of the axial and reduced cyclotron modes. Another effect of the mode coupling is that while the motions are coupled the quantum numbers of the motions equalize. Thus, one can extract a relation between the energies in each degree of freedom. Let the energies be

$$E_+ = \hbar\nu_+(n_+ + \frac{1}{2}) \tag{4.14}$$

$$E_z = \hbar\nu_z(n_z + \frac{1}{2}) \tag{4.15}$$

if $n_+ = n_z$, then

$$\frac{E_+}{E_z} = \frac{\nu_+}{\nu_z} \approx 25 \tag{4.16}$$

According with eq. 4.16 and assuming that the ion is in thermal equilibrium with the 4.2 K surrounding, it is possible to measure the reduced cyclotron frequency at a temperature of approx. $100 \text{ K} \approx 9 \text{ meV}$. Actually, the lowest axial energy that has been achieved is ≈ 60 K [Dje04]. This gives a reduced cyclotron energy of about $1500 \text{ K} \approx 100$ meV which is small if compared with the $33\,000 \text{ K} \approx 3$ eV as the minimum reduced cyclotron energy [Ver03] at which the ion is visible over the Johnson-noise of the tank circuit.

4.4   Measurement procedure

In order to measure the electronic g-factor several steps have to be performed. All of them have been described in the second and third chapter. Now they will be summarized in order to give an overview of the experiment before giving the final result. First, a single ion has to be trapped according to the procedures described in sec. 3.2. Once a single ion is prepared in the trap and all its frequencies have been measured for the first time, the procedure continues in a measurement cycle shown in the flow chart in fig. 4.7. At the end of each complete cycle, the number $n(\nu_{MW}/\nu_C)$, of spin-flips induced in the precision trap at a given frequency ratio $\Gamma = \nu_{MW}/\nu_C$ is obtained. Since the superconducting magnet has a finite stability, in the order of 10^{-9}/hour, for each cycle the given frequency ratio Γ is slightly different even without changing the irradiated microwaves frequency. This allows to probe statistically the ratio Γ in small ranges. After approximately 24h the microwave frequency ν_{MW} is changed. When enough data points, in the form $n(\Gamma)/n_{\Gamma t}$ ($n_{\Gamma t}$ is the total number
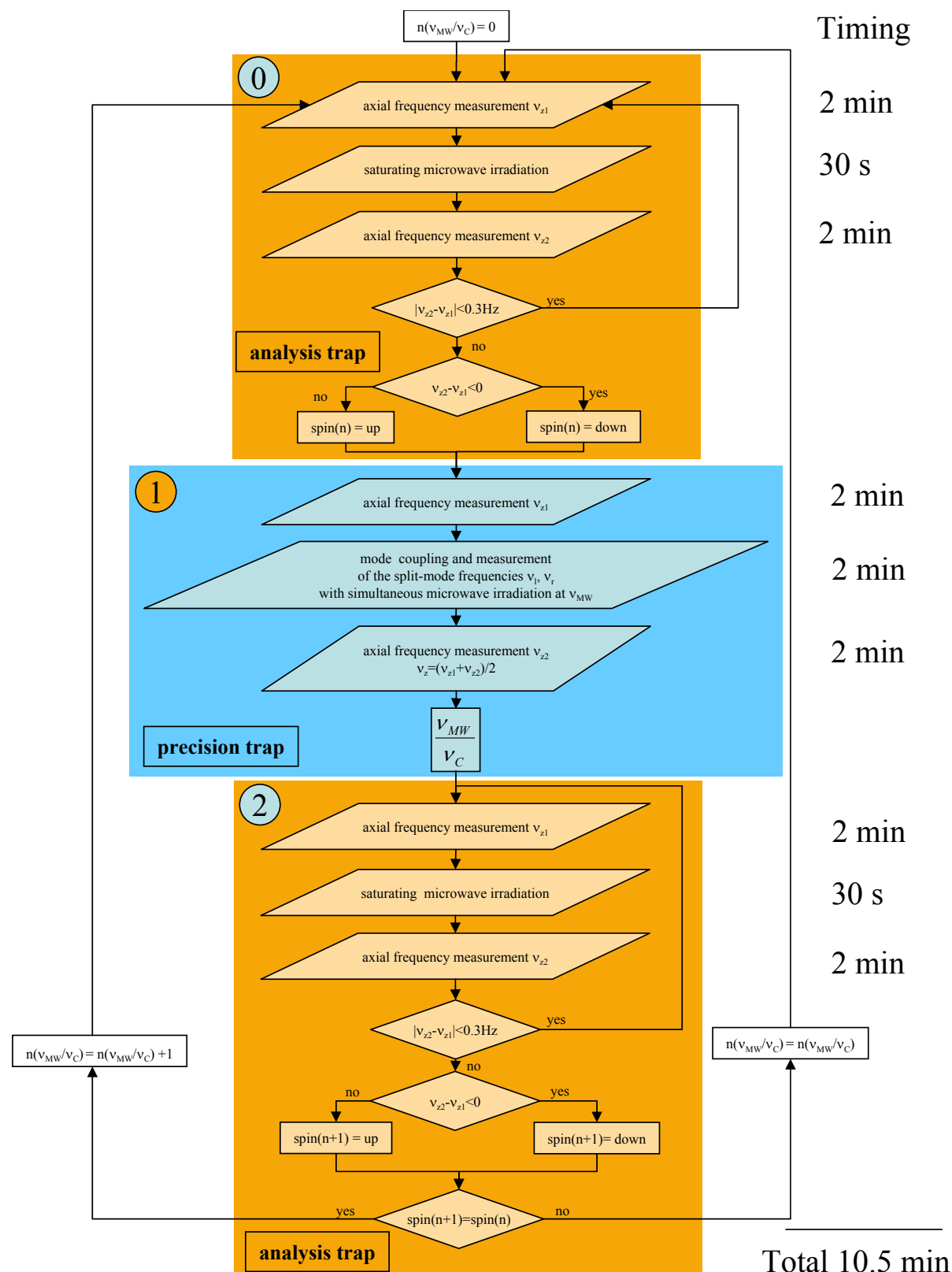
Figure 4.7: **Flow chart of the measuring process. The rhomboidal boxes indicate processes, in the square boxes are included values of variables and the diamond-shaped boxes include decisions. The different color regions denote the two different traps, 0 and 2 denote the analysis trap and 1 denotes the precision trap. In the normal measurement the sub-cycle denoted with 0 is only run once and then the cycle goes 0-1-2-1-2... In the right column the typical times for each process are given.**

of tries at the frequency ratio Γ) are collected it is possible to plot a histogram of the probability of inducing a spin-flip in the precision trap as a function of the frequency ratio Γ. Applying the measurement cycle described above, for $^{16}O^{7+}$ the resonance curve shown in fig. 4.8 was obtained. From this curve a value for Γ can be extracted. But, for producing this histogram an arbitrary bin width was used. For a high enough number of experimental data the maximum of the resonance should be independent of the bin-width used to build the histogram. In fact, as can be seen in figure 4.9, the maximum of the resonance shows a certain dependence on the bin-width. Therefore, the value for Γ that will be used to determine the g-factor is obtained by averaging the values corresponding to several different bin-widths and is found to be:

$$\Gamma_0 = 4164.376\ 184\ 3(48) \tag{4.17}$$

where the given uncertainty is obtained as an average of the statistical uncertainties of all the histograms used for calculating the average.

4.5   The electronic g-factor

Once the ν_{MW}/ν_C resonance is obtained the next step is to extract the electronic g-factor from the equation 3.5 in which the ratio q/e is known, the ratio $\frac{\nu_{MW}}{\nu_C} = \frac{\nu_{MW}}{\nu_C}$ is the quantity measured in this experiment, and the mass ratio has to be taken from
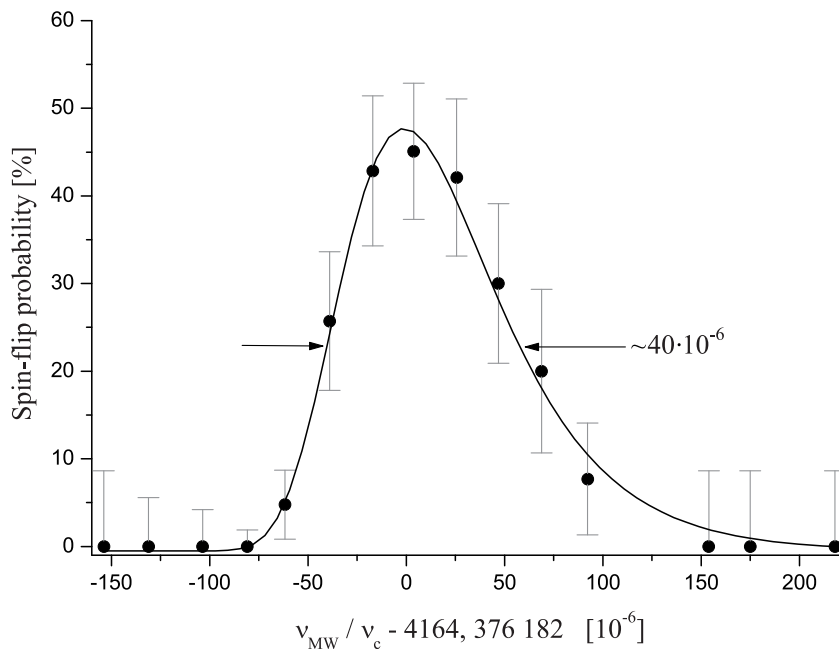
Figure 4.8: **Histogram the probability of inducing a spin-flip for a frequency ratio ν_{MW}/ν_C, also called Γ resonance. The bins are here represented as circles. The uncertainty of the bins is given by the binomial distribution. The bin width is arbitrary. The full line is a least-squares fit to** $y_0 + A exp[1 - exp(-\frac{x-x_c}{w}) - \frac{x-x_c}{w}]$ **with** $\mathbf{y_0 = -0.6 \pm 2.1}$, $A = 48 \pm 6$, $w = (40 \pm 5) * 10^{-6}$ **and** $x_c = 4164.376\ 182\ 3 \pm 0.000\ 005\ 7.$
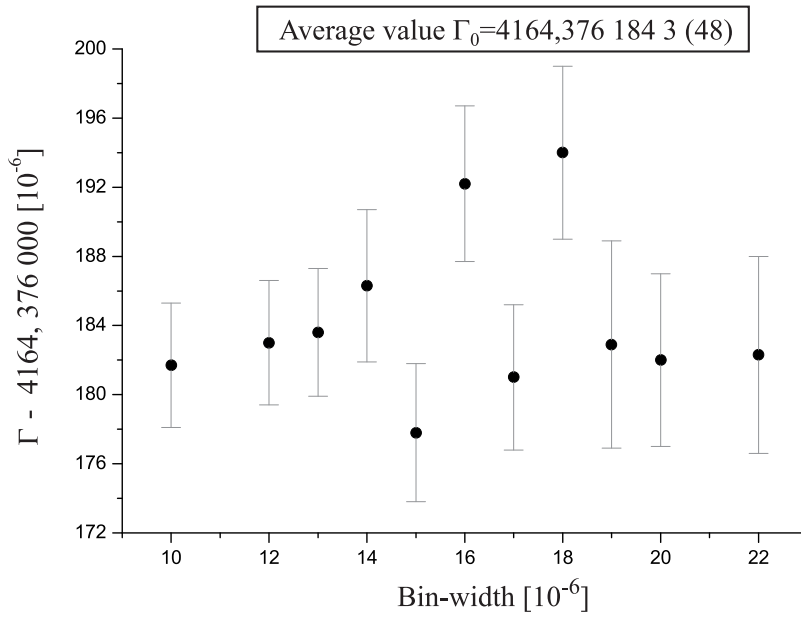
Figure 4.9: **Maximum of the Γ-resonance as a function of the chosen bin-width. As final value for obtaining the g-factor, Γ_0, the average value was taken.**

the literature. The first part of the mass ratio is the electron's mass. Its present accepted value is the one given in [Far95]

$$m_e = 0.000\ 548\ 579\ 911\ 1(12)u. \tag{4.18}$$

In the case of $^{16}O^{7+}$, the ion's mass is given by $m_i = m_O - 7m_e + E_{Bind.}$, where m_O is the atomic mass of oxygen 16 that can be found in [Aud95] and is accepted to be

$$m_O = 15.994\ 914\ 622\ 0(25)u. \tag{4.19}$$

$E_{Bind.}$ is the sum of the binding energies for all the missing electrons. From the data given in [Kel87] it can be obtained

$$E_{Bind} = 0.000\ 001\ 258\ 66(9)u. \tag{4.20}$$

4.5.1 Possible uncertainty sources

In an experimental work one has always to deal with two kind of uncertainties, first and unavoidable are the statistical errors introduced by the finite number of experimental data. The other source of uncertainty is the one introduced by the experimental setup not being perfect, which usually leads to shifts in all measured quantities. These shifts, if the source is known and understood, may be corrected. In the case of the present experiment one has to deal with several effects, the more prominent will be discussed next. In table 4.2 the leading uncertainties and systematic corrections are listed.

- Ground loop: One important feature of a Penning trap is the sensitivity of the axial frequency to changes in the static potential difference applied between the ring and the endcap electrodes. For introducing r.f.-signals a large amount of coaxial lines connecting the experimental setup with the r.f-generators is needed. The ground conductor of these coaxial lines give rise to so called ground loops, which are connections between the two main electrical grounds of the experiment, namely the magnet's enclosure and the electronic's rack. Since the coaxial cables have a finite resistance the magnetic flux fluctuations through these loops produce fluctuations in the voltage difference between these two "ground" levels. Thus, the axial frequency experiences some fluctuations. While measuring, the potential difference between the "grounds" is monitored and the influence on the axial frequency is calibrated.

- Time base: Since the g-factor is a result of a measurement of frequencies it is very important to control the stability of the internal clocks of all frequency generators and the FFT spectrum analyzer. All frequency generators (radio frequency and microwaves) are locked to a rubidium 10 MHz frequency standard which is itself locked to a Cs atomic clock through the PTB-Braunsweig radio signal. The only device that is not locked to any external time base is the FFT-analyzer which, due to internal specifications, cannot be locked. Therefore, an extra known r.f.-signal is introduced in order to correct the measured frequencies, this is the so called frequency marker (fig. 4.2).

- Extrapolation to vanishing energies and microwave amplitude: As explained in section 2.5 the shape and the center of the resonance depends on the motional energies and in the exciting microwaves amplitude. The g-factor is measured using finite energies of the motions and amplitude of the microwaves and then an extrapolation is performed to vanishing energies and microwave amplitude based on the line-shape knowledge.

- Spectral purity of the microwaves: Since the microwave generators are not ideal, the line width of microwaves is a function of their amplitude. This is another source of uncertainty in our measurement.

In addition to that, other sources of uncertainty are the ones introduced by the quantities that were obtained from the literature, the most prominent of them is the error quoted in the electron's mass (eq. 4.18). This is actually the limitation on the precision of the g-factor delivered by the present experiment.

4.5.2   Comparison of results

Combining the values in 4.17, 4.18, 4.19, 4.20 the value for the electronic g-factor is obtained and it amounts to

$$g_{exp} = 2.000\ 047\ 020\ 8(24)(44). \tag{4.21}$$

This value is in very good agreement with the theoretical result from V.M. Shabaev and V.A. Yerokhin [Yer02] which amounts to

$$g_{theo} = 2.000\ 047\ 020\ 2(6) \tag{4.22}$$

Description	Value	Uncertainty
Maximum of the resonance	4164.376 184 3	$48 \cdot 10^{7}$
Extrapolation $T_z/B_{MW} \to 0$	-0.000 007 4	$8 \cdot 10^{7}$
Extrapolation $E \to 0$	≈ 0	$6 \cdot 10^{11}$
Spectrum analyzer time base	-0.000 001 6	$1 \cdot 10^{7}$
Lorentz fit	-0.000 001 0	$4 \cdot 10^{7}$
Microwaves spectral purity	—	$2 \cdot 10^{7}$
Relativistic effects	—	$4 \cdot 10^{9}$
Ground loops	—	$4 \cdot 10^{7}$
Total	4164.376 174 3	$49 \cdot 10^{7}$

Table 4.2: **Collection of the most prominent systematic corrections to Γ and the related uncertainties. The uncertainty given to the maximum of the resonance corresponds to the statistical error in the determination of the center. The total uncertainty is obtained by quadratic sum of all components.**

and also agrees very good with the previous experimental result from Verdú *et al.* [Ver04]

$$g_{exp1} = 2.000\ 047\ 025\ 4(15)(44). \tag{4.23}$$

In both experimental results, the uncertainty is given in two parts, the first is the combined systematic and statistic uncertainty and the second (44×10^{10}) is arising from the uncertainty in the electron mass.

Chapter 5

Discussion and Outlook

> The wireless telegraph is not difficult to understand. The ordinary telegraph is like a very long cat. You pull the tail in New York, and it meows in Los Angeles. The wireless is the same, only without the cat.
>
> Albert Einstein

The experimental uncertainty

Comparing the results with the classical method (eq. 4.23) and with the new method (eq. 4.21), a bigger uncertainty can be observed in the latest. This contradicts the expectations for this new method. This effect arises mainly from a couple of factors. As this measurement on $^{16}O^{7+}$ was performed as a test of the new method some systematics were not treated carefully enough in order to accelerate the data acquisition. The main effect that can be seen in the resonance on fig. 4.8 is the asymmetry of the resonance, mainly due to the relatively high axial energy at which the measurement was performed, around 200K. This elevated axial energy is introduced on purpose in order to increase the signal/noise ratio. This increase of the axial energy leads to a broadening of the resonance (fig. 2.13).A second source for the broadening of the resonance curve is that in order to maximize the spin-flip's induction probability the microwave amplitude was set to a high value. The artificially increased line-width of the resonance is the main contribution to the statistical and systematical uncertainty since for a given number of experimental data the uncertainty increases linearly with the width of the resonance.

The determination of the electron's mass

Comparing the results of the theoretical calculation with both experimental results a very good agreement is found. Thus, repeating the measurement for several ion species if the same kind of agreement between theory and experiment is found the theoretical calculations could be believed to be accurate. Then, the result of such calculations could be used as an input in the g-factor "formula" (eq. 3.5). Using the Γ measured for $^{12}C^{5+}$ and taking into account that the definition of the atomic mass unit is

$$1u \equiv \frac{m_{^{12}C}}{12} \tag{5.1}$$

the electron's mass could be extracted. Since the electron's mass uncertainty is the main limitation to the experimental accuracy on the g-factor measurements, this determination can lead to an improvement on the electron's mass [Bei02]. Making use of the available data (carbon and oxygen) Yerokhin et al. [Yer02b] did an evaluation of the electron's mass, yielding the value

$$m_e = 0.000\ 548\ 579\ 909\ 3(3)u \tag{5.2}$$

which agrees and improves the previous accepted value [Far95] by a factor of 4

$$m_e = 0.000\ 548\ 579\ 911\ 1(12)u. \tag{5.3}$$

After the test measurement presented in section 4.5 the setup was opened to tune the cryogenic LC-circuits to the frequencies of $^{12}C^{5+}$. This change was made in order to repeat the measurement performed by Häffner et al. [Häf00b] with increased accuracy. This improvement in the experimental result may lead to an order of magnitude better accuracy on the determination of the electron's mass.

The reduction of the uncertainty in the determination of the electron's mass should have been the main result of the present work. Unfortunately, after changing the resonance frequency of the LC-circuits, creating and successfully detecting single $^{12}C^{5+}$ ions and preparing the setup for the final measurement, it was not possible to detect ions in the analysis trap. We analyzed carefully the electronics and we did not observe any anomaly. Then we observed that it was possible to transport the ions back and forth from the precision to the analysis trap. We observed that this was possible even applying voltages to the ring electrode of the analysis trap such that any positively charged particle would have escaped from the trap.
We think that this problem was caused by charging up of some dielectric material deposited on the surface of one of the electrodes. Another possibility could be some charging up of one of the electrodes that would be not connected to the external power supplies while on cryogenic temperature. All connections and voltages were checked at room temperature.
After several months of intense search for the possible source of the problem we had to give up due to economic reasons. The apparatus was opened, a new trap was designed and significant changes in the electronics were implemented. The completion of this work takes several months and goes beyond the time schedule of this thesis.

Outlook

One of the goals of the g-factor experiment is to test bound-QED effects. As shown in the first chapter these effects scale up with increasing Z. Thus, experiments on heavier ions are even more interesting for this purpose. Due to the higher ionization energies the present trap/electron-gun is not able to go much further than hydrogen-like oxygen. Therefore, a new trap has been developed and is being built up in a very similar the setup. This new trap will be able to create and store ions up to hydrogen like calcium ($^{40}Ca^{19+}$). On the other hand, a new facility, HITRAP, is being built up at the accelerator facility at GSI-Darmstadt in order to create and decelerate, cool and trap highly charged heavy ions [Qui01]. At HITRAP ions like $^{238}U^{92+}$ at

rest should be available for experiments of the same kind of the one discussed in the present work.

Other possibilities are for example measurements on series of ions of the same atom in different charge states, mainly comparisons of the g-factors of hydrogen-like and lithium like ion. This could test calculations on electron correlations.

There are also proposals [Qui04] for the measurement of the magnetic moment of the proton, and the comparison with the one of the antiproton as a test of the CPT-theorem.

For some of these new measurements a critical improvement has to be implemented. The experimental object is the spin of the particles. As explained in sec. 2.2 to be detected it has to be coupled to an external degree of freedom through a magnetic field inhomogeneity. The strength of this magnetic field inhomogeneity is limited by the ferromagnetic material's saturation of the magnetization. Therefore, the maximum attainable frequency shift (eq. 3.6) is limited and it decreases with increasing ion's mass. With the present method it would be impossible to detect it for particles like the proton because of its small magnetic moment. To overcome this problem a new method has been developed by Stahl et al. [Sta04]. With this method it is not the frequency of the motion that is measured and compared for spin up and down, but the total phase $(\nu_z \cdot t + \phi_0)$ of the motion. Then, if the initial phase ϕ_0 is controlled, a frequency shift $\delta\nu_z$ would lead to a phase shift $\delta\nu_z \cdot t + \phi_0$ that increases linearly with the waiting time between the instant when the shift occurs and the instant at which the phase is measured. Thus, if the frequency shift is too small to be measured directly, for measuring the phase shift one has only to wait long enough to let it become big enough.

List of Figures

List of Tables

Bibliography

[All87] L. Allen and J.H. Eberly
         Optical Resonance and Two-level Atoms
         Dover Publications Inc., New York (1987)

[Aud95] G. Audi and A. H. Wapstra
         The 1995 update to the atomic mass evaluation
         Nuclear Physics A **595**(1995)409

[Bei00] T. Beier
         The g_j factor of a bound electron and the hyperfine structure splitting in
         hydrogenlike ions
         Phys. Rept. **339** (2000) 79

[Bei02] T. Beier *et al.*
         New Determination of the Electron's Mass
         Phys. Rev. Lett. **88** (2002) 011603-1

[Bre28] G. Breit
         Nature (London) **122** (1928) 649

[Bro86] L.S. Brown and G. Gabrielse
         Geonuim Theory: Physics of a single electron or ion in a Penning trap.
         Rev. Mod. Phys. **58** (1986) 233

[Cor90] E. A. Cornell *et al.*
         Mode coupling in a Penning trap: π pulses and classical avoided crossing.
         Phys. Rev. A **41** (1990) 312

[Dal85] J. Dalibard and C. Cohen-Tannoudji
         Dressed-atom approach to atomic motion in laser light:
         the dipole force revisited.
         J. Opt. Soc. Am. B, **2** (1985) 1707

[Deh68] H.G. Dehmelt and F.L. Walls
         "Bolometric" Technique for the rf spectroscopy of stored ions.
         Phys. Rev. Lett. **21** (1968) 127

[Dje04] S. Djekic *et al.*
         The Temperature of a single ion in a Penning trap.
         Submitted to Eur. Phys. Jour. D

[Deh86] Hans Dehmelt
Continuous Stern-Gerlach effect: Noise and the measurement process
Proc. Natl. Acad. Sci. USA **83** (1986) 3074

[Deh87] Robert S. Van Dyck, Jr., Paul B. Schwinberg, and Hans G. Dehmelt
New High-Precision Comparison of Electron and Positron g Factors
Phys. Rev. Lett. **59** (1987) 26

[Far95] Dean L. Farnham, Robert S. Van Dyck, Jr., and Paul B. Schwinberg
Determination of the Electron's Atomic Mass and the Proton/Electron Mass
Ratio via Penning Trap Mass Spectroscopy
Phys. Rev. Lett. **75** (1995) 3598

[Gab89] G. Gabrielse *et al.*
Open-endcap Penning Traps for High Precision Experiments.
Int. J. Mass Spectrom. Ion Processes , **88** (1989) 319

[Häf98] Hartmut Häffner
Präparation einzelner hochgeladener Ionen in einer Penningfalle
Diplomarbeit Mainz (1998)

[Häf00] Hartmut Häffner
Präzisionmessung des magnetischen Moments des Elektrons in wasserstof-
fänlichem Kohlenstoff
Dissertation, Universität Mainz (2000)

[Häf00b] H. Häffner *et al.*
High-Accuracy Measurement of the Magnetic Moment Anomaly of the Elec-
tron Bound in Hydrogenlike Carbon
Phys. Rev. Lett. **85** (2000) 5308

[Her96] Nikolaus Hermanspahn
Aufbau eines Tieftemperaturkryostaten zum Betrieb einer Penningfalle
Diplomarbeit Mainz (1996)

[Her99] Nikolaus Hermanspahn
Das magnetische Moment des gebundenen Elektrons in wasserstoffänlichem
Kohlenstoff (C^{5+})
Dissertation, Universität Mainz (1999)

[Her00] N. Hermanspahn *et al.*
Observation of the Continuous Stern-Gerlach Effect on an Electron Bound
in an Atomic Ion
Phys. Rev. Lett. **84** (2000) 427

[Hug99] V. Hughes and T. Kinoshita
Anomalous g values of the electron and muon
Rev. Mod. Phys.**71** (1999) S133

[Im98] Marcel Immel
Aufbau einer Mikrowellenapparatur zur Spectroskopie an einzelnen gespe-
icherten Ionen
Diplomarbeit Mainz (1998)

[Joh80] C.E. Johnson, H.G. Robinson
gJ Factor of an Ion: Determination of $g_J(^4He^+, 1^2S_{1/2})/g_J(^4He, 2^3S_1)$
Phys. Rev. Lett. **45** (1980) 250

[Kel87] Raymond L. Kelly
Atomic and Ionic Spectrum Lines below 2000 Angstroms: Hydrogen through
Krypton
J. Phys. Chem. Ref. Data, **16**, S1 (1987)1

[Kin90] T. Kinoshita
Theory of the anomalous magnetic moment of the electron
numerical approach.
Quantum Electrodynamics, T. Kinoshita (Ed.), World Scientific, Singapur
(1990)

[Qui01] W. Quint *et al.*
HITRAP: A Facility for Experiments with Trapped Highly Charged Ions
Hyperfine Interactions **132**(2001)457

[Qui04] W. Quint *et al.*
Continuous Stern-Gerlach effect and the magnetic moment of the antiproton
Nucl. Inst. Meth. B **214** (2004) 207

[Sak85] J.J. Sakurai
Modern Quantum Mechanics
Addison-Wesley Publishing Company Inc. (1994)

[Sta98] Stefan Stahl
Aufbau eines Experimentes zur Bestimung elektronischer g-Faktoren einzel-
net wasserstoffänlichen Ionen
Dissertation, Universität Mainz (1998)

[Sta04] S. Stahl *et al.*
Phase sensitive measurement of small frequency differences.
Publication in preparation

[Sch51] J. Schwinger
On gauge invariance and vacuum polarization
Phys. Rev. **82** (1951) 664

[Sch54a] J. Schwinger
Theory of quantized fields. V
Phys. Rev. **93** (1954) 615

[Sch54b] J. Schwinger
Theory of quantized fields. VI
Phys. Rev. **94** (1954) 1362

[See98] P. Seelig *et al.*
Ground State Hyperfine Splitting of Hydrogenlike $^{207}Pb^{81+}$ by Laser Exci-
tation of a Bunched Ion Beam in the GSI Experimental Storage Ring
Phys. Rev. Lett. **81** (1998) 4824

[Tie77] J.S. Tiedeman, H.G. Robinson
         Determination of $g_J(^1H, 1^2S_{1/2})/g_s(e)$: Test of Mass-Independent Correc-
         tions
         Phys. Rev. Lett. **39** (1977) 602

[Tön96] M. Tönges
         Aufbau einer Mikrowellenanlage zur Spektroskopie an wasserstoffänlichen
         Ionen in einer Penningfalle.
         Diplomarbeit Mainz (1996)

[Ver03] José Verdú Galiana
         Ultrapräzise Messung des Electronischen g-Faktors in wasserstoffänlichem
         Sauerstoff
         Dissertation, Universität Mainz (2003)

[Ver04] J. Verdú *et al.*
         Electronic g Factor of Hydrogenlike Oxigen ^{16}O^{7+}
         Phys. Rev. Lett. **92** (2004) 093002-1

[Yer02] V.M. Shabaev and V.A. Yerokhin
         Recoil Correction to the Bound-Electron g Factor in H-Like Atoms to All
         Orders in αZ
         Phys. Rev. Lett. **88** (2002) 901801-1

[Yer02b] V.A. Yerokhin, P. Indelicato, and V.M. Shabaev
         Self-Energy Correction to the Bound-Electron g Factor in H-like Ions
         Phys. Rev. Lett. **89** (2002) 143001-1

[Win75] D.J. Wineland and H.G. Dehmelt
         Principles of the stored ions calorimeter.
         Jour. Appl. Phys. **46** (1975) 919

[Win99] H. Winter *et al.*
         Bound Electron g-Factor in Hydrogen-Like Bismuth.
         U. Grundinger (ed.), GSI Report 99-1, GSI, Darmstadt, Germany. (1999)
         p.87

Acknowledgements

Lebenslauf

Persönliche Daten
Name: Valenzuela Salazar
Vorname: Tristán
Geburtsdatum: 6. Januar 1973
Geburtsort: Saint Maurice, Frankreich
Staatsangehörigkeit: Spanisch
Familienstand: Ledig
Wohnort: Mainz, Deutschland
tel(priv.):   +49-6131-
tel(uni):   +49-6131-
fax: +49-6131-
e-mail:

Schulausbildung und Studium

1979-1980	Grundschule Rajoletes, Sant Joan d'Alacant, Spanien
1980-1981	Spanische Grundschule Paris, Frankreich
1981-1982	Grundschule Rajoletes, Sant Joan d'Alacant
1982-1983	Spanische Grundschule Paris
1983-1987	Grundschule Rajoletes, Sant Joan d'Alacant
1987-1988	Spanisches Gymnasium *Lycée Espagnol de Paris*, Frankreich
1988-1992	Gymnasium Sant Joan d'Alacant
Juni 1992	Abitur:
	Selectividad an der *Universitat d'Alacant*, Alacant, Spanien
Sept. 1999	Spanisches Diplom der Physik an der *Universitat de València*, Spanien
Feb. 2001	Diplomarbeit:
	Collective oscillation of an electron cloud confined in a Penning trap
	unter Betreuung von Prof. G. am Institut für Physik
	der Johannes-Gutenberg-Universität Mainz, Deutschland
2000-2004	Wissenschaftlicher Mitarbeiter
	in der Arbeitsgruppe
	Institut für Physik der Johannes-Gutenberg-Universität Mainz

Abschlüsse

9/1999	*Licenciado en Física* (Spanisch Diplom Physiker)
2/2001	Deutscher Diplomarbeit